Species barrier as molecular basis for adaptation of synthetic prions with N-terminally truncated PrP

Human Rezaei, Davy Martin, Laetitia Herzog, Fabienne Reine, Alba Marín Moreno, Mohammed Moudjou, Naima N. Aron, Angélique Igel, Hannah Klute, Stella Youssafi, et al.

▶ **To cite this version:**

Human Rezaei, Davy Martin, Laetitia Herzog, Fabienne Reine, Alba Marín Moreno, et al.. Species barrier as molecular basis for adaptation of synthetic prions with N-terminally truncated PrP. FEBS Journal, 2024, 291 (22), pp.5051-5076. ⟨10.1111/febs.17291⟩. ⟨hal-04766015⟩

HAL Id: hal-04766015

https://hal.inrae.fr/hal-04766015v1

Submitted on 22 May 2025

HAL is a multi-disciplinary open access archive for the deposit and dissemination of scientific research documents, whether they are published or not. The documents may come from teaching and research institutions in France or abroad, or from public or private research centers.

L'archive ouverte pluridisciplinaire **HAL**, est destinée au dépôt et à la diffusion de documents scientifiques de niveau recherche, publiés ou non, émanant des établissements d'enseignement et de recherche français ou étrangers, des laboratoires publics ou privés.

Distributed under a Creative Commons CC BY-NC-ND 4.0 - Attribution - Non-commercial use - No Derivative Works - International License

Check for updates

The FEBS Journal

FEBS PRESS science publishing by scientists

Species barrier as molecular basis for adaptation of synthetic prions with N-terminally truncated PrP

Human Rezaei[1], Davy Martin[1], Laetitia Herzog[1], Fabienne Reine[1], Alba Marín Moreno[1], Mohammed Moudjou[1], Naima Aron[2], Angélique Igel[1], Hannah Klute[1], Stella Youssafi[1], Jean-Baptiste Moog[1], Pierre Sibille[1], Olivier Andréoletti[2], Joan Torrent[1,3] and Vincent Béringue[1]

1 Université Paris-Saclay, INRAE, UVSQ, VIM, Jouy-en-Josas, France
2 INRAE, ENVT, IHAP, Toulouse, France
3 INM, Univ Montpellier, INSERM, CNRS, France

Keywords
evolution; prion; species barrier; strains; synthetic

Correspondence
V. Béringue and H. Rezaei, INRAE, Université Paris-Saclay, Domaine de Vilvert, UMR0892 VIM, Jouy-en-Josas 78 350, France
Tel: +33 1 34 65 26 00
E-mail: vincent.beringue@inrae.fr and human.rezaei@inrae.fr

Laetitia Herzog and Fabienne Reine contributed equally to this article.
Human Rezaei and Vincent Béringue shared senior authorship.

(Received 26 February 2024, revised 4 July 2024, accepted 24 September 2024)

doi:10.1111/febs.17291

Mammalian prions are neurotropic pathogens formed from PrP^{Sc} assemblies, a misfolded variant of the host-encoded prion protein PrP^{C}. Multiple PrP^{Sc} conformations or strains self-propagate in host populations or mouse models of prion diseases, exhibiting distinct biological and biochemical phenotypes. Constrained interactions between PrP^{Sc} and PrP^{C} conformations confer species specificity and regulate cross-species transmission. The pathogenicity of fibrillar assemblies derived from bacterially expressed recombinant PrP (rPrP) has been instrumental in demonstrating the protein-only nature of prions. Yet, their ability to encode different strains and transmit between species remains poorly studied, hampering their use in exploring structure-to-strain relationships. Fibrillar assemblies from rPrP with hamster, mouse, human, and bovine primary structures were generated and tested for transmission and adaptation in tg7 transgenic mice expressing hamster PrP^{C}. All assemblies, except the bovine ones, were fully pathogenic on the primary passage, causing clinical disease, PrP^{Sc} brain deposition, and spongiform degeneration. They exhibited divergent adaptation processes and strain properties upon subsequent passage. Assemblies of hamster origin propagated without apparent need for adaptation, those of mouse origin adapted abruptly, and those of human origin required serial passages for optimal fitness. Molecular analyses revealed the presence of endogenously truncated PrP^{Sc} species in the resulting synthetic strains that lack the 90–140 amino acid region considered crucial for infectivity. In conclusion, rPrP assemblies provide a facile means of generating novel prion strains with adaptative/evolutive properties mimicking genuine prions. The PrP amino acid backbone is sufficient to encode different strains with specific adaptative properties, offering insights into prion transmission and strain diversity.

Abbreviations
AFM, atomic force microscopy; BSE, bovine spongiform encephalopathy; CJD, Creutzfeldt–Jakob disease; CNS, central nervous system; GdnHCl, guanidine hydrochloride; GPI, glycosylphosphatidylinositol; Ha, hamster; HMW, high molecular weight; Hu, human; IMW, intermediate molecular weight; LMW, low molecular weight; Mo, mouse; PIRIBS, parallel-in-register intermolecular β-sheet; PK, proteinase K; PMCA, protein misfolding cyclic amplification; rPrP, recombinant PrP; RT-QuIC, real-time quacking-induced conversion; SD, seeding dose; TME, transmissible mink encephalopathy.

This is an open access article under the terms of the Creative Commons Attribution-NonCommercial-NoDerivs License, which permits use and distribution in any medium, provided the original work is properly cited, the use is non-commercial and no modifications or adaptations are made.

Introduction

In mammals, the mature form of the cellular prion protein (PrP^C) is mainly expressed in the central nervous system (CNS). PrP^C is a monomeric, ~210 amino acids long, glycosylphosphatidylinositol (GPI)-anchored membrane glycoprotein with high structural identity across mammalian species. The disordered N terminus contrasts with the folded C terminus, which comprises three α-helices and a short antiparallel β-sheet [1,2]. Prions, constitutively, are abnormally folded conformations of PrP^C (termed PrP^{Sc}) with infectious properties. The misfolding process involves refolding in all regions but the N terminus, leading to increased β-sheet content and the formation of multiple assemblies with respect to their secondary to quaternary structures (for reviews [3–5]). PrP^{Sc} self-replicates by templating the conversion and polymerization of PrP^C in the CNS, causing fatal neurodegenerative diseases like Creutzfeldt–Jakob disease (CJD) in humans, scrapie in sheep and goats, bovine spongiform encephalopathy (BSE) in cattle and chronic wasting disease in cervids [6]. PrP transgenic modeling and cell-free conversion assays indicate that most mammalian PrP^C can convert into PrP^{Sc}, with the lowest convertible species being dog, horse, and rabbit PrP^C [7–10].

Multiple prion strains coexist within the same host population, each exhibiting unique biological properties. These strain-specific characteristics include disease duration (the time between infection and disease onset or terminal stage), the nature of clinical signs, and the spatial distribution of both PrP^{Sc} deposits and spongiform vacuolation in the CNS. These traits are heritable under defined transmission conditions and are encoded within structurally distinct conformers of PrP^{Sc} [3,11], as revealed by biochemical analyses and direct Cryo-EM analyses of purified PrP^{Sc}. In these experiments, while PrP^{Sc} adopted a common parallel-in-register intermolecular β-sheet (PIRIBS)-based core architecture, notable variations were observed in the folding of the C-terminal domain [12–14]. The strain-specific relationship between PrP^{Sc} fold and disease phenotype remains poorly understood. Adding another layer of complexity is the evidence for the accumulation of more than one PrP^{Sc} conformer in the brain during disease pathogenesis. Within a single strain, there is evidence for a larger diversity of PrP^{Sc} conformations [15–20], varying significantly in their specific infectivity [3,21], due to a deterministic, highly dynamic, diversification process during the replication [22]. The physiopathological role, if any, of each PrP^{Sc} subset remains to be clarified. Remarkably, the strain phenotype is encoded in subpopulations as small as dimers of PrP^{Sc} [23].

Interspecies transmission of prions can occur, exemplified by the emergence of variant CJD in the human population dietary exposed to BSE prions. Interspecies transmission is typically limited by a species or transmission barrier, the magnitude of which depends critically on both the infecting strain type and the conformational landscape of the recipient host PrP^C. Conceptually, if one of the infecting PrP^{Sc} conformers within the strain aligns with the portfolio of conformations foreign PrP^C can adopt in the PrP^{Sc} state, there will be little or no transmission barrier. Experimentally, in transgenic mouse models expressing heterotypic PrP—considered among the most relevant for studying prion transmission barriers [3,24–26]—propagation will thus occur at full attack rate on primary passage, with minimal reduction of disease duration and limited evolution of the strain phenotype on subsequent passages. If not, transmission will not occur or be less efficient, resulting in a low attack rate, prolonged incubation times, or asymptomatic disease on primary passage. Achieving full pathogenicity, stabilized incubation times and neuropathological phenotypes will then necessitate serial passaging. However, this can sometimes occur abruptly at the second passage, a phenomenon referred to as prion 'mutation' because variants with new strain properties suddenly emerge [27–29]. Adaptation may not occur when conditions remain unfavorable, a phenomenon called 'non adaptative prion amplification' or transient prion replication [8]. Homotypic PrP transmissions generally appear to lack a transmission barrier. Nonetheless, evidence suggests the possible emergence of new strain types, due to preferential selection of substrains or mutational events, akin to heterotypic transmissions [30–33].

The main theoretical model describing prion cross-species adaptation is the 'conformational selection' model [34,35]. Grounded in the concept of best replicator selection [36], this model considers the existence of structurally heterogenous PrP^{Sc} assemblies within a prion strain or isolate. Cross-species transmission favors the selection of the best PrP^{Sc} replicator either because it pre-exists as an integral part of what defines a prion strain or because it is generated *de novo*, such as by complementation between structurally distinct PrP^{Sc} assemblies [37]. A 'deformed templating' variant of this model has been developed to account for the *in vivo* evolutionary process of certain recombinant prions [38]. The basic assumption of this variant

17424658, 2024, 22, Downloaded from https://febs.onlinelibrary.wiley.com/doi/10.1111/febs.17291 by Université de Versailles-Saint-Quentin-en-Yvelines, Wiley Online Library on [22/05/2025]. See the Terms and Conditions (https://onlinelibrary.wiley.com/terms-and-conditions) on Wiley Online Library for rules of use; OA articles are governed by the applicable Creative Commons License

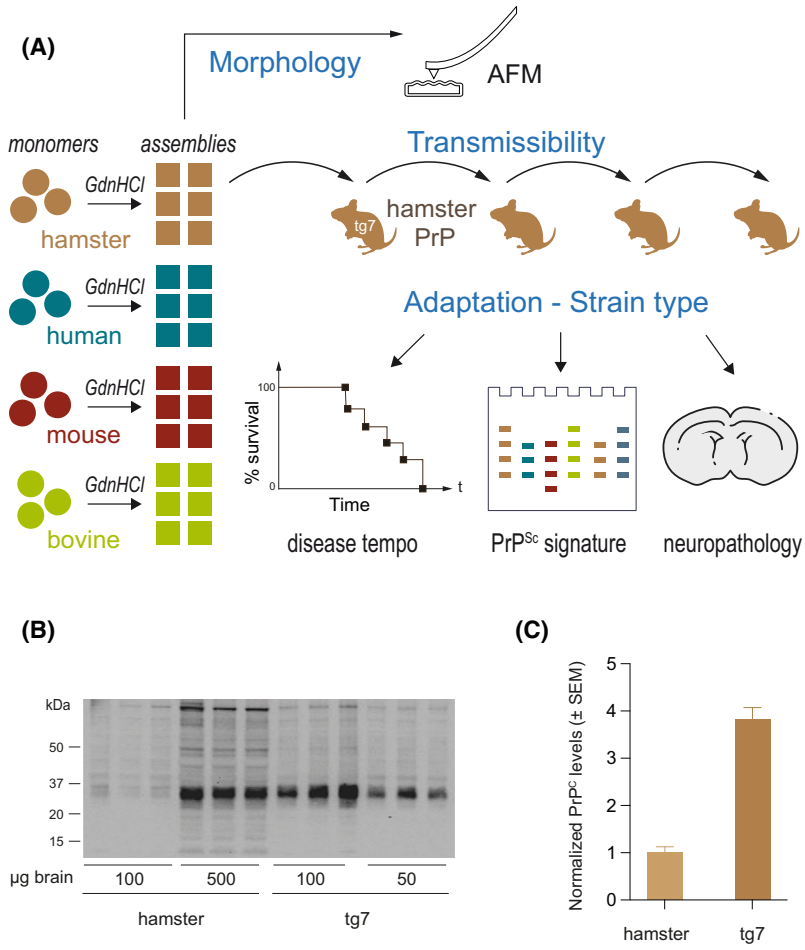

Fig. 1. Schematic of the recombinant PrP assemblies bioassay and details of the transgenic mice used to characterize their transmission properties. (A) Scheme describing the strategy adopted to generate the recombinant PrP (rPrP) assemblies in chaotropic conditions (guanidine hydrochloride, GdnHCl) and characterize their transmission/strain properties in transgenic mice expressing hamster PrP (tg7 line) over passaging. The color code used for the rPrP assemblies is used throughout all figs. (B, C) PrP^{C} overexpression levels in tg7 mouse brain. (B) Detection by immunoblot (Sha31 antibody) and (C) quantification of PrP^{C} expression levels in the brains of hamster PrP mice (tg7 line) and golden Syrian hamsters. Quantification was performed on immunoblots with $n = 3$ animals. Results are expressed as mean levels ± SEM.

is the absence of initial PrP assemblies heterogeneity, compensated by the creation of heterogeneity on initial passages in the new host, based on the templating interface misfit between PrP^{Sc} and host PrP^{C}. Altered PrP^{Sc} conformers may be initially generated on primary passage and outcompeted by the best replicant on serial adaptation.

In direct support of the protein-only nature of prions, there exists a global consensus regarding the *bona fide* infectivity/proteopathic activity of bacterially-derived recombinant PrP (rPrP) refolded *in vitro* into amyloid fibrils [39–46]. Prions resulting from the experimental infection of laboratory rodents or PrP transgenic mice with rPrP fibrils are termed synthetic prions. However, generating fully pathogenic synthetic prions often required additional brain co-factors and/or prior PrP^{Sc}-seeded amplification through chemically defined processes using protein misfolding cyclic amplification (PMCA) [47–52] or technologically optimized variants thereof [53,54]. Given these challenges, the capacity of pure rPrP amyloid fibrils (i.e., those made without co-factors and/or no prior amplification) to generate different synthetic prion strains [41,46] has seldom been addressed, and their abilities to cross PrP transmission have been explored even less frequently.

In this study, we examined the transmission properties of pure rPrP fibrils obtained from four distinct mammalian species in transgenic mice expressing homotypic or heterotypic PrP. All but one species exhibited full pathogenicity. Additionally, we observed the selection of three distinct synthetic prion strains, with their adaptation characterized by either a straightforward process or dominance of a species barrier, crossed through mutational events or requiring multiple passages.

Results

The general strategy employed in this study is schematized in Fig. 1A. Recombinant PrP amyloid-like preparations from hamster ($rPrP^{Ha}$), human ($rPrP^{Hu}$),

17424658, 2024, 22, Downloaded from https://febs.onlinelibrary.wiley.com/doi/10.1111/febs.17291 by Université de Versailles-Saint-Quentin-en-Yvelines, Wiley Online Library on [22/05/2025]. See the Terms and Conditions (https://onlinelibrary.wiley.com/terms-and-conditions) on Wiley Online Library for rules of use; OA articles are governed by the applicable Creative Commons License

mouse ($rPrP^{Mo}$), and bovine ($rPrP^{Bo}$) primary structures were generated in partially unfolding conditions (Materials and methods and Fig. S1). Their morphological characterization was conducted using techniques such as atomic force microscopy (AFM). Their transmission properties, capacity to adapt and strain-specified characteristics were investigated through four iterative passages in hamster PrP transgenic mice (tg7 line), thus involving both homotypic PrP and heterotypic PrP transmission contexts. Tg7 mice overexpress 4-fold PrP^{C} in the brain (Fig. 1B,C). This model, routinely used in our laboratory for prion

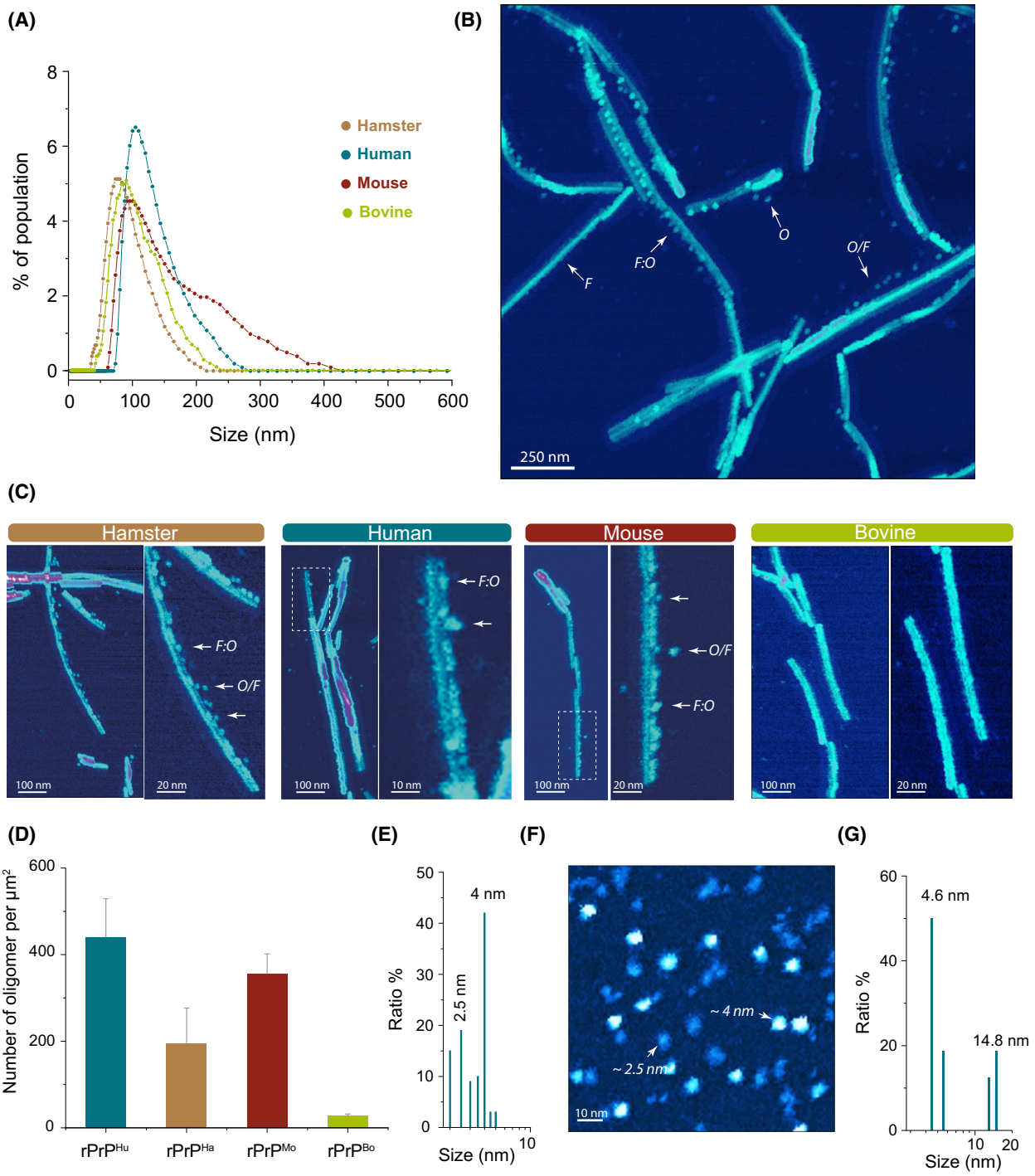

17424658, 2024, 22, Downloaded from https://febs.onlinelibrary.wiley.com/doi/10.1111/febs.17291 by Université de Versailles-Saint-Quentin-en-Yvelines, Wiley Online Library on [22/05/2025]. See the Terms and Conditions (https://onlinelibrary.wiley.com/terms-and-conditions) on Wiley Online Library for rules of use; OA articles are governed by the applicable Creative Commons License

Fig. 2. Quaternary structure characterization of mouse, hamster, human, and bovine recombinant PrP assemblies. (A) Size distribution of the recombinant PrP (rPrP) assemblies, as estimated by dynamic light scattering (DLS). The mean average hydrodynamic radius ranged between 100 and 150 nm. (B) Representative images of mouse rPrP assemblies by atomic force microscopy (AFM). Multiple types of organization were identified; fibrillar assemblies (*F*), fibrillar assemblies in interaction with oligomeric species (*F:O*), oligomers at the fibrils vicinity (*O/F*) and isolated oligomers (*O*). (C) Representative AFM images of human, mouse, hamster and bovine rPrP assemblies. Note the morphological heterogeneity for human, mouse and hamster species with presence of fibrillar and spherical (arrows) assemblies. (D) Number of spherical objects per μm^2 estimated for the four rPrPs assemblies preparation which served for inoculation. The statistics were performed by estimating the number of spherical objects on four different AFM fields of 500×500 nm. The data were then normalized to 1 μm^2. Results are expressed as number of oligomers per surface ± SD. (E) Size distribution of the spherical objects from $rPrP^{Ha}$ assembly preparation. Two distinct sizes of spherical objects can be observed. (F) Representative AFM image of spherical objects enriched by ultracentrifugation, highlighting the presence of the two oligomeric populations. (G) Fibril height distribution from $rPrP^{Ha}$ assembly preparation. Two distinct sets of fibrils can be observed. The AFM images shown are representative of $n = 46$ (mouse), $n = 60$ (hamster), $n = 35$ (human, bovine) images analyzed from one (bovine) or two batches of rPrP assemblies inoculated to tg7 mice.

structural and transmission studies, has been instrumental in previous research [15,37,55–58]. There is no evidence for spontaneous disease or infectivity in these mice, based on a history of over 1000 mice inoculated with foreign prions (whether of natural or laboratory origin) or prion-free tissue extracts ([37,56] and V. Béringue, unpublished data).

Coexistence of fibrillar and oligomeric assemblies in interaction in the rPrP preparations

The rPrP assemblies were characterized for their size distribution, mean average molecular weight and morphology. As shown in Fig. 2A, for all the four species, the dynamic light scattering analyses of the assemblies revealed a mean hydrodynamic size distribution between 100 and 150 nm. The ultra-structure and morphology analyses of the assemblies by AFM using a 10 Å nominal cantilever revealed an overall fibrillar shape (Fig. 2B,C). However, in the case of $rPrP^{Ha}$, $rPrP^{Hu}$, and $rPrP^{Mo}$ fibrillar preparations, numerous spherical objects were observed. The bovine assemblies differed from the other three by a lower abundance of these spherical objects; the estimation of the number of spherical objects per μm^2 suggested that their population in $rPrP^{Bo}$ is less compared to $rPrP^{Ha}$, $rPrP^{Hu}$ and $rPrP^{Mo}$ assemblies (Fig. 2D). These spherical objects were either staked on the fibrils as protrusions or at vicinity or occasionally as isolated objects (Fig. 2B,C). Measurements of the mean average Z-sizes of the spherical objects, as typically estimated from $rPrP^{Ha}$, suggested that two distinct sets of spherical objects were present: one of 25 Å, the other of 40 Å (Fig. 2E). By comparison, the size of monomeric recombinant PrP is approximatively 12 Å. These two types of spherical objects were morphologically distinct by AFM (Fig. 2F). These observations indicate that the spherical objects are oligomeric states of PrP. Notably, measurements of the mean fibril heights also indicated that two distinct sets of fibrils were present in the $rPrP^{Ha}$ assemblies preparations (Fig. 2G).

Altogether, this morphological characterization highlights the existence of constitutional structural heterogeneity for $rPrP^{Ha}$, $rPrP^{Hu}$ and $rPrP^{Mo}$ assemblies, with the coexistence of at least two types of fibrillar and oligomeric assemblies. Furthermore, AFM images tend to suggest that the oligomeric species specifically interact with the fibrillar component. By considering the coexistence of multiple types of assemblies in interaction within the preparation, the term assembly rather than amyloid fibrils will be then used in the following.

Efficient transmission of hamster, mouse, and human rPrP assemblies to tg7 mice

We inoculated groups of tg7 mice with 10 µg of rPrP assemblies by intracerebral route. As negative controls, tg7 mice were inoculated with hamster, mouse, and human rPrP monomers (10 µg). None of the mice inoculated with the monomers exhibited any signs of disease over > 700 days post-inoculation (Table S1). Concerning the rPrP assemblies, all groups, except for those inoculated with the $rPrP^{Bo}$, developed a symptomatic neurological disease (Table 1). The clinical phase was protracted compared to laboratory-adapted hamster prions such as 263K/Sc237, 139H or ME7-H (4–6 weeks vs. 3–7 days, [15,37,58]). Waddling gait, weight loss, kyphosis, and progressive hindlimb paralysis were observed in the three groups. Intense scraping and pruritus were noticed in tg7 mice inoculated with $rPrP^{Ha}$ and $rPrP^{Hu}$ assemblies.

On primary passage, $rPrP^{Ha}$/$rPrP^{Mo}$, and $rPrP^{Hu}$ assemblies achieved 100% and ~90% attack rates, respectively. The mean disease durations were ~280 days for $rPrP^{Ha}$, ~345 days for $rPrP^{Mo}$ and

17424658, 2024, 22, Downloaded from https://febs.onlinelibrary.wiley.com/doi/10.1111/febs.17291 by Université de Versailles-Saint-Quentin-en-Yvelines, Wiley Online Library on [22/05/2025]. See the Terms and Conditions (https://onlinelibrary.wiley.com/terms-and-conditions) on Wiley Online Library for rules of use; OA articles are governed by the applicable Creative Commons License

Table 1. Serial transmission of hamster, mouse, human, and bovine rPrP assemblies to tg7 mice by intracerebral route.

	Mean survival in days ± SEM (n/n_0)[a]			
rPrP assemblies	Hamster	Mouse	Human	Bovine
1st passage	282 ± 17 (9/9)	346 ± 10 (10/10)	476 ± 11 (8/9)	574 ± 47 (0/10)
2nd passage	273 ± 12 (8/8)	84 ± 1 (8/8)	260 ± 16 (8/8)	661 ± 40 (0/10)
3rd passage	244 ± 13 (8/8)	84 ± 2 (7/7)	215 ± 7 (6/6)	
4th passage	238 ± 15 (5/5)	80 ± 2 (6/6)	219 ± 7 (8/8)	

[a] n/n_0, number of mice with neurological disease and positive for PrP^{res} in the brain by immunoblotting/number of inoculated mice.

~480 days for $rPrP^{Hu}$ (Table 1). Subsequently generated batches of rPrP assemblies, 4 years later, were 100% pathogenic, with disease durations consistent with the initial observations for $rPrP^{Ha}$ and $rPrP^{Mo}$, and slightly longer (though not significant) for $rPrP^{Hu}$ (Fig. 3A). This observation suggests deterministically governed processes in the conversion of monomeric rPrP into pathogenic assemblies.

For $rPrP^{Bo}$, the second passage performed with a pool of brains from primary passage remained negative. For $rPrP^{Ha}$, $rPrP^{Mo}$ and $rPrP^{Hu}$, three subpassages were performed with brains from individual, sick mice to investigate potential transmission barriers or low infectivity issues (Table 1). With $rPrP^{Ha}$ assemblies, the mean disease duration on the second passage was close to that seen on primary passage and decreased modestly over further passaging to reach ~240 days at the 4th passage. Conversely, with $rPrP^{Mo}$ assemblies, the mean disease duration abruptly decreased on the second passage and stabilized at ~80 days. With $rPrP^{Hu}$ assemblies, the mean disease duration decreased to reach ~220 days at the 3rd passage where it stabilized. Except for $rPrP^{Mo}$ assemblies, the clinical phase remained prolonged on subpassaging of $rPrP^{Ha}$ and $rPrP^{Hu}$ assemblies.

Altogether, one rPrP assemblies ($rPrP^{Bo}$) was not transmissible to tg7 mice and three were fully pathogenic, with their disease duration evolution suggestive of faithful propagation ($rPrP^{Ha}$) or distinct adaptation processes ($rPrP^{Mo}$ and $rPrP^{Ha}$). Based on the final disease durations, it is anticipated that at least two different synthetic prion strains emerged—one derived from mouse rPrP assemblies, and the other from hamster/human assemblies.

Seeding activity of rPrP-derived prions

The real-time quacking-induced conversion (RT-QuIC) assay is based on PrP^{Sc}-seeded polymerization and conversion of rPrP substrate into a thioflavin T-positive amyloid conformation [59]. It enables rapid and highly sensitive detection of prions and, in an endpoint dilution mode, titration of their seeding activity. It serves as a quantitative proxy for infectivity titrations through endpoint dilution in animal bioassays [60].

We first compared the initial seeding activity of the rPrP assemblies to check whether the absence of disease in tg7 mice inoculated with $rPrP^{Bo}$ was due to a lack of converting capacity. Serial 10-fold dilutions of the rPrP assemblies were added to the RT-QuIC reaction mixture containing human rPrP as substrate and subjected to the assay. The Spearman–Kärber method was used to estimate the seeding dose (SD) per mL in which 50% of the replicate reactions are thioflavin T-positive (SD_{50}). As shown in Fig. 4A, the SD_{50} values of the assemblies were all within the same range, between, $10^{13.9}$ and $10^{14.9}$ SD_{50} per mL of a 20 μM solution. Thus, $rPrP^{Bo}$ assemblies were not discrepant.

We next estimated the relative concentrations of prion seeding activity of $rPrP^{Ha}$-, $rPrP^{Hu}$- and $rPrP^{Mo}$-derived synthetic prions in tg7 mouse brains to assess any change in the seeding activity over passaging and adaptation and compared the final values to those of the 263K hamster prion strain in tg7 mice. As shown in Fig. 4B, the SD_{50} per mL of 10% brain homogenate values were consistent over passaging, regardless of the rPrP assemblies transmitted. At the fourth passage, brains from tg7-$rPrP^{Ha}$ and tg7-$rPrP^{Hu}$ showed positive replicates down to the $10^{-6}/10^{-7}$ dilution, and those from tg7-$rPrP^{Mo}$ brains down to the 10^{-5} dilution. In comparison, with 263K, the last positive dilution established $10^{-6}/10^{-7}$ (Fig. 4C). The seeding activities of the synthetic prions were thus equivalent or 100-fold lower than those of hamster-adapted 263K scrapie prions. The lag phase of the RT-QuIC reactions was shortened with the synthetic prions compared to 263K, particularly at the lowest dilutions (Fig. 4C). Similar results were obtained when hamster rPrP replaced human rPrP as substrate in the RT-QuIC reactions (Fig. 4D). Therefore, while the number of seeding-competent particles is comparable or lower between synthetic prions and 263K in tg7 brains, the conversion rate/speed per particle is higher in the former.

17424658, 2024, 22, Downloaded from https://febs.onlinelibrary.wiley.com/doi/10.1111/febs.17291 by Université de Versailles-Saint-Quentin-en-Yvelines, Wiley Online Library on [22/05/2025]. See the Terms and Conditions (https://onlinelibrary.wiley.com/terms-and-conditions) on Wiley Online Library for rules of use; OA articles are governed by the applicable Creative Commons License

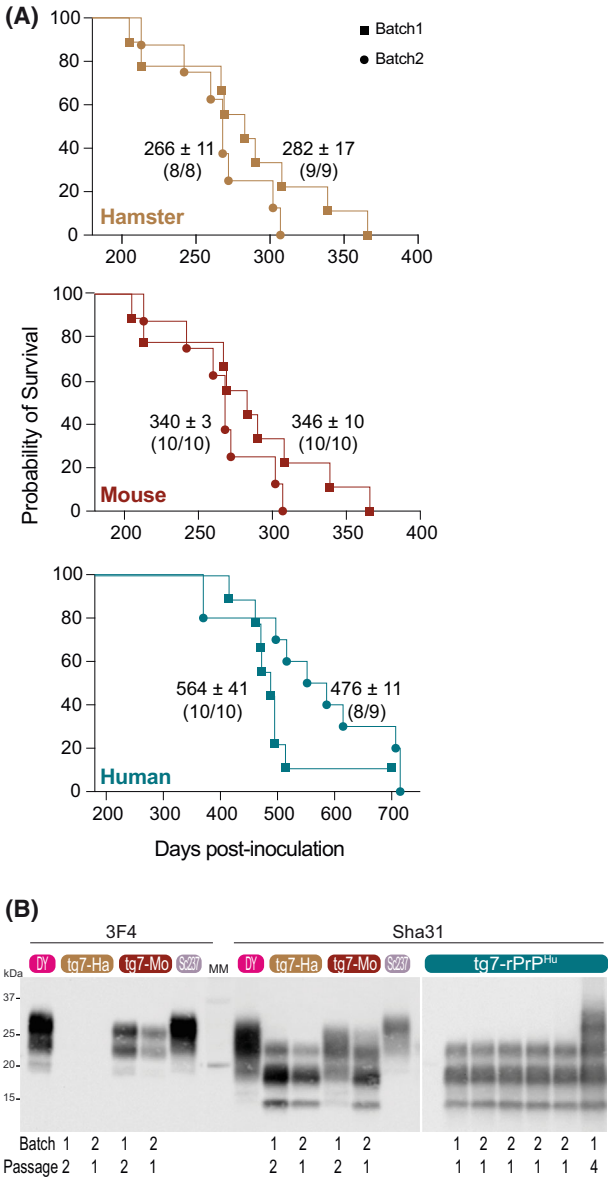

Fig. 3. Distinct batches of hamster, mouse and human recombinant PrP assemblies are pathogenic in tg7 mice. (A) Kaplan–Meier curve plotting the percentage of mice without prion disease (probability of survival) against the incubation time (days post-inoculation). Square symbol refers to the inoculated batch 1 (Table 1). Circle symbol refers to the inoculated batch 2, prepared independently with a 4-year interval. The survival curves for batch 1 and batch 2 were not statistically significantly different (logrank test). The survival times, expressed as mean ± SEM days, and in parenthesis the number of diseased, PrP^{res}-positive/number of inoculated mice are indicated for each batch. (B) Electrophoretic pattern of PrP^{res} in the brains of tg7 mice inoculated with different batches of assemblies from hamster (Ha), mouse (Mo) or human (Hu) recombinant PrP. The 3F4 and Sha31 monoclonal anti-PrP antibodies were used to detect full-length and truncated PrP^{res} bands (see Fig. 5). Tg7-passaged Sc237 and DY PrP^{res} are shown as control. MM: molecular mass markers. The western blot shown is representative of three independent experiments, and $n = 6$ (batch 1) and $n = 5$ (batch 2) mouse brains analyzed.

To be noted, RT-QuIC reactions seeded with aged, uninfected tg7 brain dilutions as negative controls remained thioflavin T negative up to 25 h with human and hamster rPrP substrates (Fig. 4C,D), indicating no spontaneous conversion of the substrates and the absence of spontaneously forming, seeding-competent PrP in tg7 mice.

Recombinant PrP assemblies induce differing PrP^{res} patterns in tg7 mouse brains

To characterize the strain properties of the $rPrP^{Ha}$-, $rPrP^{Hu}$-, and $rPrP^{Mo}$-derived synthetic prions, we examined the electrophoretic signature of proteinase K (PK)-resistant PrP^{Sc} (PrP^{res}) in the brains of the diseased mice. All analyzed brains accumulated substantial levels of PrP^{res}, regardless of the rPrP species inoculated and the number of passages. The electrophoretic profiles were atypical compared to prototypical Sc237 PrP^{res} and varied among the three rPrP species inoculated.

In tg7-$rPrP^{Ha}$ brains, PrP^{res} was characterized by the presence of three bands from ~15 to ~23 kDa, over four passages (Fig. 5A, top panel). This banding pattern was resolved into a single band migrating at ~15 kDa (Fig. 5A, middle panel) after deglycosylation with PNGase, suggesting variable glycosylation, similar to Sc237 PrP^{res}, but ~5 kDa shorter in size. The monoglycosylated isoform was dominant. Mice infected with the second batch of $rPrP^{Ha}$ assemblies showed a similar low molecular weight (LMW) PrP^{res} banding pattern in the brain (Fig. 3B), indicating an invariance in the banding pattern as the function of the batch.

In tg7-$rPrP^{Hu}$ brains over three passages, The PrP^{res} banding pattern resembled that of tg7-$rPrP^{Ha}$, but at the 4th passage, a second PrP^{res} product of higher molecular weight (HMW) appeared in all analyzed mice ($n = 4$; Figs 5A and 3B with the second batch). After deglycosylation, this band migrated slightly faster than Sc237 PrP^{res} (Fig. 5A). Therefore, tg7-$rPrP^{Hu}$ prions and tg7-$rPrP^{Ha}$ prions differed, despite overlapping final disease durations in tg7 mice.

In tg7-$rPrP^{Mo}$ brains, PrP^{res} displayed both LMW and HMW bands in variable proportions (Fig. 5A). After deglycosylation, an additional product of intermediate molecular weight (IMW), migrating at

17424658, 2024, 22, Downloaded from https://febs.onlinelibrary.wiley.com/doi/10.1111/febs.17291 by Université de Versailles-Saint-Quentin-en-Yvelines, Wiley Online Library on [22/05/2025]. See the Terms and Conditions (https://onlinelibrary.wiley.com/terms-and-conditions) on Wiley Online Library for rules of use; OA articles are governed by the applicable Creative Commons License

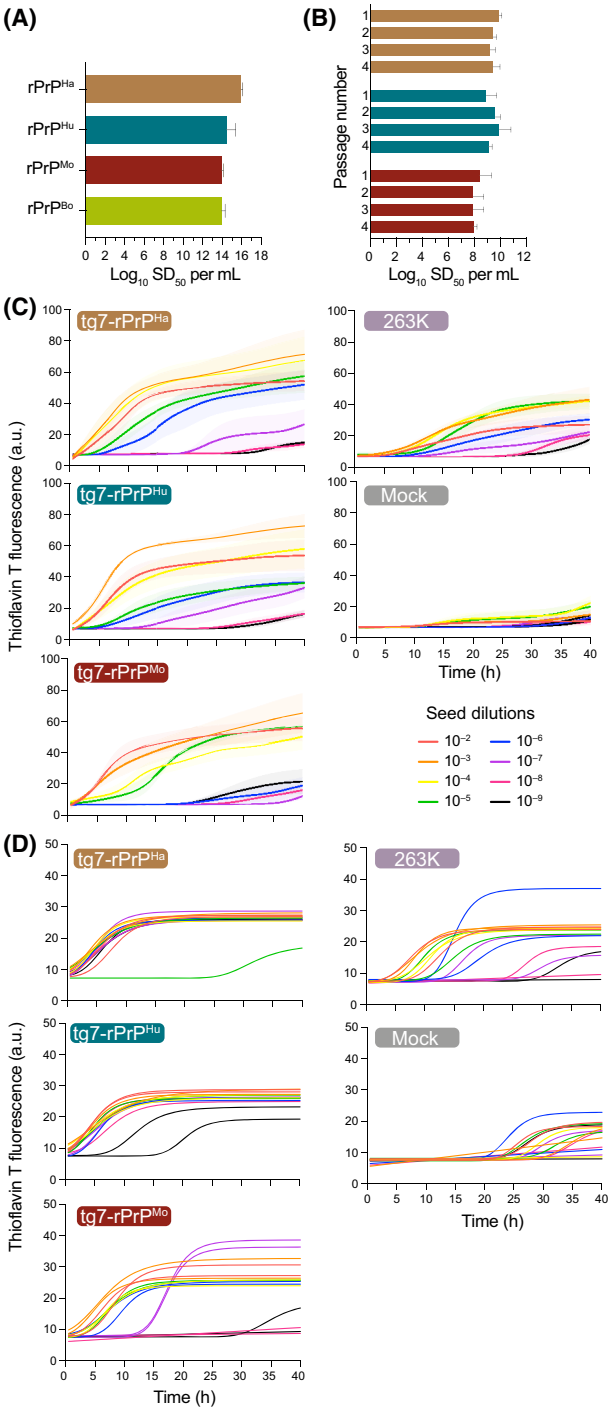

Fig. 4. Seeding activity of recombinant PrP-derived synthetic prions. (A, B) Graphs plotting (A) the seeding activity 50 (SD_{50}) per mL of 20 μM solution from the inoculated recombinant PrP (rPrP) assemblies, (B) the SD_{50} per mL of 10% (w/v) homogenates from tg7-rPrP^{Ha}, tg7-rPrP^{Hu} and tg7-rPrP^{Mo} mice at passage 1 to 4, as estimated by the Spearman–Kärber method from the real-time quacking-induced conversion (RT-QuIC) reactions using serial dilutions of rPrP assemblies or brain homogenates as seeds and human rPrP as substrate. The results shown have been obtained from $n = 4$ (A) to $n = 8$ (B) replicates. (C) RT-QuIC reactions with dilutions (colored, as indicated) of brain homogenates from tg7-rPrP^{Ha}, tg7-rPrP^{Hu} and tg7-rPrP^{Mo} mice at the 4th passage. As positive control, brain homogenates from tg7 mice inoculated with 263K hamster prions were used. As negative control, brain homogenates from aged, uninfected tg7 mice were used. Each trace is the fitted curve plotting the mean ± SEM thioflavin T fluorescence intensity over time (recorded every 30 min) from $n = 5$ (tg7-rPrP^{Hu}, tg7-rPrP^{Mo}) to $n = 10$ (tg7-rPrP^{Ha}, 263K, mock) independent replicates. (D) Individual RT-QuIC reactions obtained hamster rPrP with dilutions (colored, as indicated) of brain homogenates from tg7-rPrP^{Ha}, tg7-rPrP^{Hu} and tg7-rPrP^{Mo} mice at the 4th passage. As positive control, brain homogenates from tg7 mice inoculated with 263K hamster prions were used. As negative control, brain homogenates from aged, uninfected tg7 mice were used. Each brain sample was serially diluted down to the 10^{-9} dilution. Each trace is the fitted curve plotting thioflavin T fluorescence intensity over time (recorded every 30 min). RT-QuIC reactions were done in duplicates.

~16 kDa, was detected (Fig. 5A). The heterogeneity in PrP^{res} signatures persisted with the second batch of rPrP^{Mo} assemblies (Fig. 3B).

To further resolve the PrP^{res} banding patterns specific to each assembly inoculated, we performed an epitope mapping with anti-PrP antibodies spanning the PrP amino acid sequence from the PK-cleavage sites to the C terminus (Fig. 5B, Table S2). The LMW PrP^{res} bands were not detected when immunoblots were probed with antibodies with epitopes spanning the PK-cleavage sites up to residues ~130 (Fig. 5C, left column). The LMW PrP^{res} bands were detected by antibodies with epitopes spanning the central part of PrP up to the C-terminus (Fig. 5C, right column). With these antibodies but Sha31, a doublet LMW band migrating at ~14 kDa was detected (Fig. 5C, right column and A, bottom panel). We estimated that the ~15 and ~14 kDa LMW PrP^{res} fragments would have a sequence starting from position 140–145 and 150–155 up to the C terminus, respectively (Fig. 5D).

The HMW PrP^{res} bands in tg7-rPrP^{Mo} and tg7-rPrP^{Hu} brains were detected with all the anti-PrP antibodies tested. However, the HMW^{Mo} and HMW^{Hu} PrP^{res} bands differed, with the former mostly disappearing with 12B2 antibody and migrating slightly faster than the latter with the other antibodies (Fig. 5C). This suggested that HMW^{Mo} PrP^{res} was slightly more N-terminally truncated than HMW^{Hu} PrP^{res}, beyond PK-cleavage site at position 89–90, with HMW^{Hu} starting at position ~90 and HMW^{Mo} starting at position ~93 (Fig. 5D).

17424658, 2024, 22, Downloaded from https://febs.onlinelibrary.wiley.com/doi/10.1111/febs.17291 by Université de Versailles-Saint-Quentin-en-Yvelines, Wiley Online Library on [22/05/2025]. See the Terms and Conditions (https://onlinelibrary.wiley.com/terms-and-conditions) on Wiley Online Library for rules of use; OA articles are governed by the applicable Creative Commons License

The IMW PrP^{res} band in tg7-$rPrP^{Mo}$ brains was not positive with N-terminal anti-PrP antibodies, indicating truncation between amino acid positions 130 and 140 (Fig. 5B–D).

In summary, systematic PrP^{res} typing allows differentiating of prions of hamster, human, and mouse rPrP origin, revealing three distinct prion strains in tg7 mice. The coexistence of several proteolytic fragments, particularly in the case of tg7-$rPrP^{Hu}$ and tg7-$rPrP^{Mo}$, indicates a substantial degree of structural heterogeneity in their respective PrP^{res} assemblies, irrespective of the strain disease tempo in mice.

LMW PrP^{Sc} is mostly endogenously truncated

To investigate the origin of the N-terminally truncated LMW PrP^{Sc} fragments observed in immunoblots, tg7-$rPrP^{Ha}$, tg7-$rPrP^{Hu}$ and tg7-$rPrP^{Mo}$ brain homogenates (2nd and 4th passage) were treated with thermolysin to determine if these fragments pre-existed or resulted from partial digestion of full-length PrP^{Sc} by PK. For multiple prion strain/host PrP combinations, including hamster PrP, limited digestion with thermolysin completely degrades PrP^{C} while leaving $>80\%$ of PrP^{Sc} as full-length form [61–63]. Mock-infected brain homogenates from tg7 mice were treated with thermolysin as a control for efficient digestion of PrP^{C}, and Sc237-infected tg7 brain homogenates were used as a positive control. After SDS/PAGE electrophoresis, immunoblots were revealed with anti-PrP antibodies with epitopes before or after PK-cleavage sites (Fig. 5B, Table S2), to detect full-length PrP^{Sc} and full-length + truncated PrP^{Sc}, respectively. As shown in Fig. 6A, no signal was detected in uninfected brain homogenates, suggesting complete enzymatic digestion of PrP^{C}. Sc237-PrP^{Sc} was mostly detected as full-length PrP^{Sc}, inferred from the presence of SAF34-positive signal and the faint, extended pattern seen with both Sha31 and SAF84 antibodies. Low levels of full-length PrP^{Sc} were detected in thermolysin-digested PrP^{Sc} from tg7-$rPrP^{Ha}$ brains (2nd and 4th passage) and from tg7-$rPrP^{Hu}$ brains at the 2nd passage. The protein was primarily found as LMW truncated forms, including the doublet band. Thermolysin-digested PrP^{Sc} from tg7-$rPrP^{Hu}$ brains at the 4th passage and tg7-$rPrP^{Mo}$ brains yielded a stronger SAF34 positive signal, suggesting an enriched presence of full-length PrP^{Sc}. Collectively, these data indicate that the LMW PrP^{Sc} species are mostly truncated prior to PK digestion.

To distinguish between two hypotheses, i.e., whether LMW PrP^{Sc} fragments result from *in vitro* sensitivity to thermolysin or *in vivo* to endogenous proteolytic cleavage [64], the PrP^{Sc} electrophoretic pattern in the same brain homogenates was analyzed by sedimentation assay without any protease treatment. Immunoblots were revealed with anti-PrP antibodies targeting the central core of PrP to check for full-length + truncated PrP^{Sc}. As shown in Fig. 6B, a faint signal was detected in pelleted uninfected brain homogenates, suggesting limited insolubility of PrP^{C}. Sc237-PrP^{Sc} was mostly detected as the full-length form. Sedimentable PrP^{Sc} species from tg7-$rPrP^{Ha}$ and tg7-$rPrP^{Hu}$ brains were mostly detected as LMW truncated forms, with a minor component of monoglycosylated dominant full-length PrP^{Sc} (i.e., different from the signal observed in uninfected brain). PrP^{Sc} from tg7-$rPrP^{Mo}$ brains was predominantly found as full-length PrP^{Sc}. These data suggest that LMW PrP^{Sc} fragments are mostly endogenously truncated. Whether this occurs through an endogenous degradative process post full-length PrP^{C} conversion or due to straight conversion of prionogenic PrP^{C} fragment(s) of shorter size remains to be determined [65,66].

Neuropathological features of recombinant PrP-derived prions

The neuroanatomical distribution of PrP^{res} was studied by histoblotting at the 4th passage, a stage where incubation times were stabilized (Fig. 7). Brains from tg7-$rPrP^{Ha}$ and tg7-$rPrP^{Hu}$ mice exhibited a similar pattern with widespread LMW PrP^{res} deposition in several brain regions, including the cerebral cortex, thalamus, and brain stem. Several white matter tracts, such as the corpus callosum, external capsule, cingulum, optic and olfactory tracts, showed strong positive signals. The deposition in these tracts was more visible at 3rd passage with fewer contaminated brain areas (Fig. 8). In tg7-$rPrP^{Mo}$ brains, SAF84 antibody detected low levels of PrP^{res}, primarily in these white matter tracts (Figs 7 and 8), suggesting overlapping deposition of LMW PrP^{res} forms among the three synthetic strains. The 3F4 antibody, which specifically detected HMW^{Mo} PrP^{res}, showed a deposition pattern broadly overlapping with LMW PrP^{res}, suggesting absence of specific (e.g., truncated) PrP^{C} substrate converted into LMW PrP^{res} at the resolution of the histoblots.

To complete the analysis, vacuolar lesion profiles were established at every passage by histological examination (Fig. 9A). Spongiform degeneration was more severe and widespread in tg7-$rPrP^{Ha}$, tg7-$rPrP^{Hu}$, and tg7-$rPrP^{Mo}$ brains as compared to tg7-Sc237 mice. The spatial variability of the brain lesion profile was limited on subpassaging for the three synthetic strains. tg7-$rPrP^{Ha}$ and tg7-$rPrP^{Hu}$ lesion profiles were

17424658, 2024, 22, Downloaded from https://febs.onlinelibrary.wiley.com/doi/10.1111/febs.17291 by Université de Versailles-Saint-Quentin-en-Yvelines, Wiley Online Library on [22/05/2025]. See the Terms and Conditions (https://onlinelibrary.wiley.com/terms-and-conditions) on Wiley Online Library for rules of use; OA articles are governed by the applicable Creative Commons License

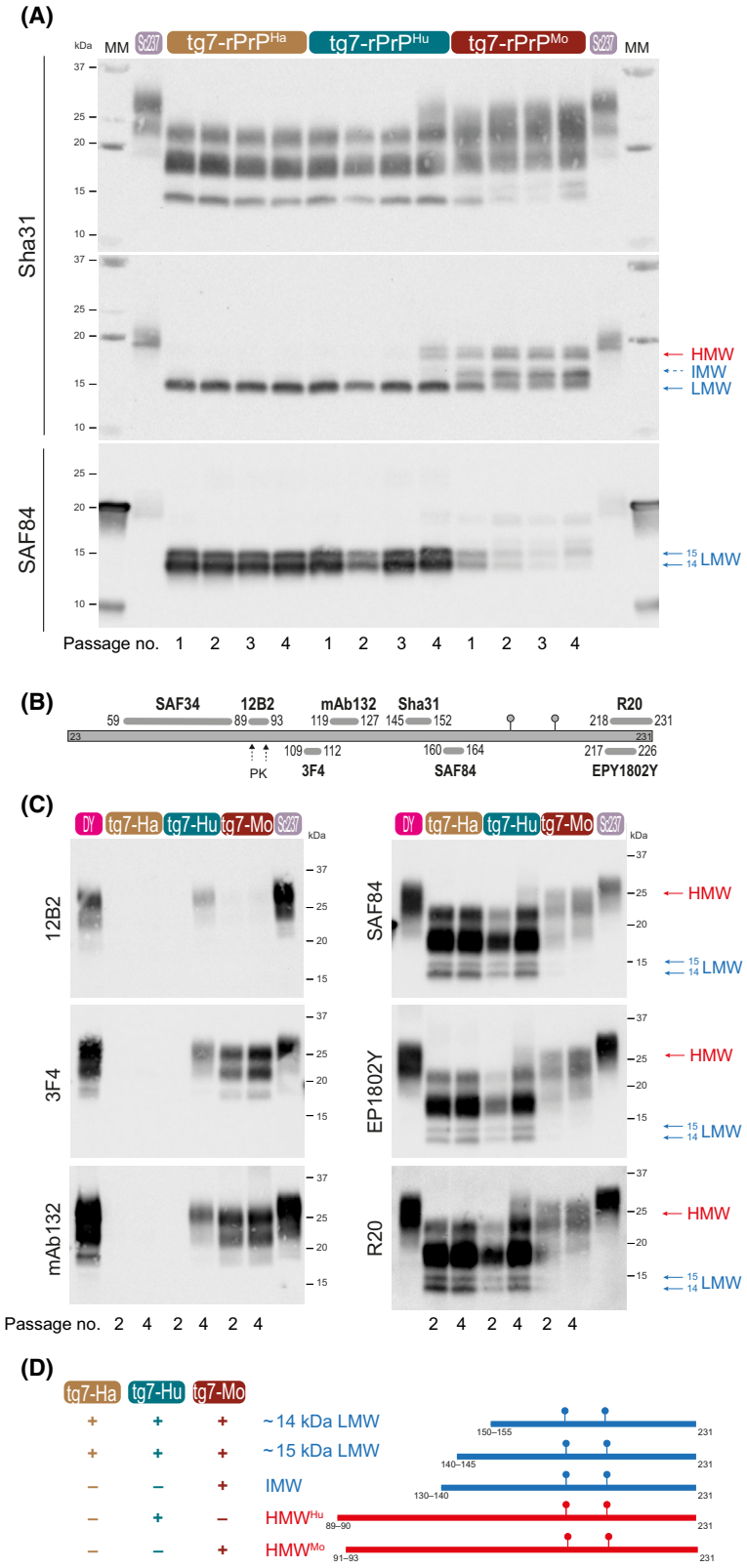

The FEBS Journal **291** (2024) 5051–5076 © 2024 The Author(s). *The FEBS Journal* published by John Wiley & Sons Ltd on behalf of Federation of European Biochemical Societies.

17424658, 2024, 22, Downloaded from https://febs.onlinelibrary.wiley.com/doi/10.1111/febs.17291 by Université de Versailles-Saint-Quentin-en-Yvelines, Wiley Online Library on [22/05/2025]. See the Terms and Conditions (https://onlinelibrary.wiley.com/terms-and-conditions) on Wiley Online Library for rules of use; OA articles are governed by the applicable Creative Commons License

Fig. 5. Biochemical properties of PrP^{res} from recombinant PrP-derived synthetic prions. (A) Immunoblots of PK-treated brain samples from tg7-$rPrP^{Ha}$, tg7-$rPrP^{Hu}$ and tg7-$rPrP^{Mo}$ mice at passage 1 to 4 as indicated. Sc237 PrP^{res} in tg7 mouse brain is shown as control. PrP^{res} pattern is shown before (top panel) and after (middle and bottom panels) deglycosylation by PNGase. Immunoblots were probed with Sha31 and SAF84 anti-PrP monoclonal antibodies as indicated. (B, C) Immunoblots at 2nd and 4th passage with anti-PrP monoclonal antibodies as indicated. Their epitopes are depicted in the schematic diagram (B). As controls, PrP^{res} from tg7-passaged Sc237 and DY prions were used. HMW, IMW and LMW PrP^{res} (15 and 14 kDa forms) are indicated by arrows. MM: molecular mass markers. The western blots shown are representative of three independent experiments, and $n = 6$ (passage 1 and 2) and $n = 4$ (passage 3 and 4) mouse brains analyzed. (D) Inventory at the 4th passage and estimation of the size of the PrP^{res} fragments according to the epitopes of the antibodies that detected these fragments, their relative migration in immunoblots and considering the average weight of one amino acid and the size of PrP GPI anchor.

relatively similar, with the intensity of vacuolation increasing on subpassaging. Intense areas of vacuolation were observed in the cortex and hippocampus, accompanied by visible neuronal loss. tg7-$rPrP^{Mo}$ lesion profile was different, with no evidence of neuronal loss (Fig. 9B).

Collectively, these data indicate that rPrP assemblies triggered prion-specific neuropathological stigmata, from the primary passage onwards. They also differentiate synthetic tg7-$rPrP^{Mo}$ prions from tg7-$rPrP^{Ha}$ and tg7-$rPrP^{Hu}$ prions. Finally, they support the view that LMW PrP^{Sc} species that propagate solely in tg7-$rPrP^{Ha}$ prions are fully pathogenic *per se*.

Recombinant PrP-derived prions convert hamster PrP substrate from Syrian hamsters by PMCA

PMCA can expedite intraspecies prion transmissions and maintain prion strains properties [57,67], offering a time-efficient and ethically sound alternative to *in vivo* investigations. We thus used this technology as a surrogate to examine whether rPrP-derived prions would propagate in hamsters. Brain lysates from Syrian hamsters and tg7 mice were seeded with serial 1:3 dilutions of tg7-rPrP synthetic prions at the 4th passage (and at the 2nd one for tg7-$rPrP^{Hu}$) and submitted to 4 serial rounds of PMCA, as described in the Materials and methods. As positive control, tg7-263K prions were used. The amplified products were treated with proteinase K and analyzed by western blotting for the presence of PrP^{res} using Sha31 antibody. When $PrP^{0/0}$ brain lysates were used as substrate, no PrP^{res} was detected, indicating absence of residual PrP^{res} from the tg7-rPrP seeds after four rounds of PMCA (Fig. 10A). Both tg7 mouse and hamster brains amplified 263K prions until the 10^{-7} dilution. Due to PrP^{C} overexpression, the amount of PrP^{res} was greater in tg7-amplified products (Fig. 10A). Both substrates allowed amplification of tg7-$rPrP^{Hu}$ (passages 2 and 4) and tg7-$rPrP^{Ha}$ prions over the range of dilutions tested, while both barely amplified tg7-rPP^{Mo} prions. Similar to 263K, the amount of generated PrP^{res} was greater with tg7 substrate (Fig. 10A). The fact that tg7 mice and hamsters react similarly in PMCA reactions supports the view that rPrP-derived synthetic prions would propagate in hamsters. Interestingly, using SAF84 by western blot showed that the PrP^{Sc} species generated by PMCA barely contained LMW species (Fig. 10B). This observation supports the hypothesis that the LMW truncations observed *in vivo* occur through endogenous degradative processes post full-length PrP^{C} conversion, the proteolytic process being inactive in the PMCA conversion assay.

Discussion

The concept of strains—defined as varying conformations of misfolded protein assemblies that elicit specific pathological manifestations in the affected host—originated with prion diseases and has been extended to other protein misfolding neurodegenerative diseases such as Alzheimer's and Parkinson's diseases [68]. Recombinant forms of the pathogenic proteins or peptides are increasingly employed to study the relationships between protein conformation and pathology, as well as the underlying strain diversity across the spectrum of these disorders (for reviews [69–71]). Paradoxically, in the prion field, very few studies have addressed the strain diversity and evolution of recombinant PrP assemblies, particularly those from crude preparations. This was investigated here with fibrillar rPrP assemblies differing in their primary structure on serial passage to a common transgenic mouse model expressing hamster PrP^{C}. The findings revealed that chaotropic treatment of monomeric rPrP from different species generated distinct prion strains. The adaptation process of these synthetic prions appeared to be primarily governed by a species or transmission barrier. Their biochemical characterization indicated the presence of an endogenous truncated C-terminal PrP^{Sc} fragment, either alone or in combination with classical PrP^{Sc}. This observation suggests that the beginning of

17424658, 2024, 22, Downloaded from https://febs.onlinelibrary.wiley.com/doi/10.1111/febs.17291 by Université de Versailles-Saint-Quentin-en-Yvelines, Wiley Online Library on [22/05/2025]. See the Terms and Conditions (https://onlinelibrary.wiley.com/terms-and-conditions) on Wiley Online Library for rules of use; OA articles are governed by the applicable Creative Commons License

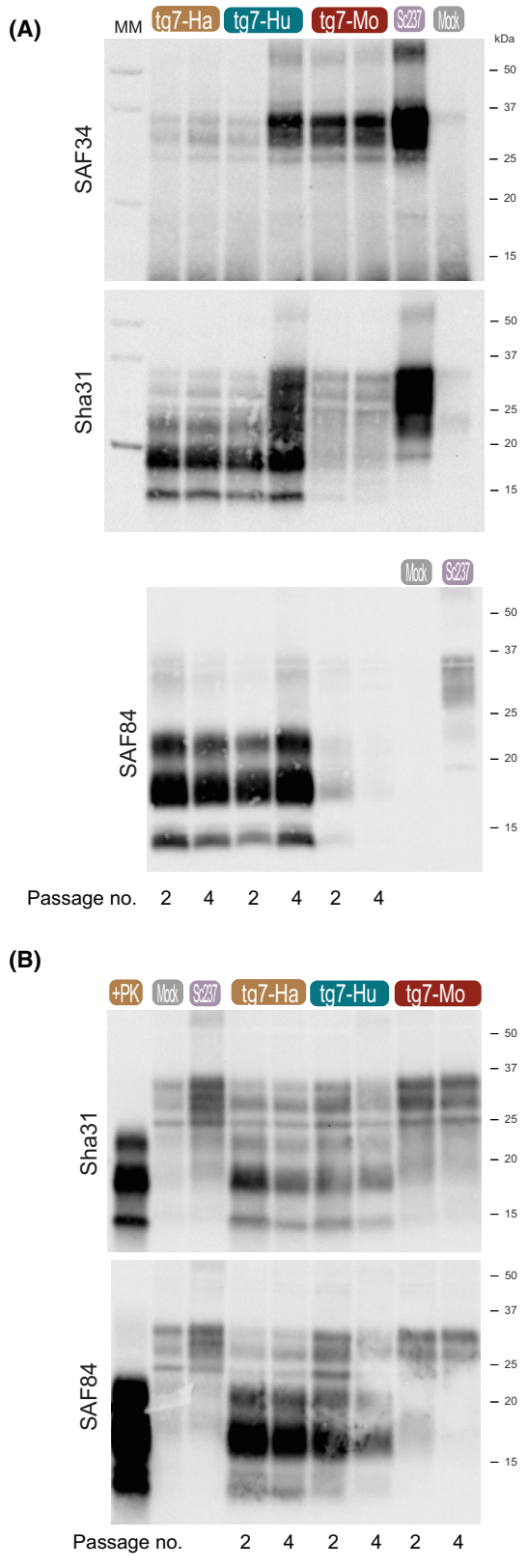

Fig. 6. Thermolysin-resistance and insolubility of PrP^{Sc} from recombinant PrP-derived synthetic prions. Immunoblots of (A) thermolysin-resistant PrP^{Sc}, (B) insoluble PrP^{Sc} from tg7-$rPrP^{Ha}$, tg7-$rPrP^{Hu}$ and tg7-$rPrP^{Mo}$ mice at passage 2 and 4 as indicated. As controls, thermolysin-digested or ultracentrifuged brain homogenates from Sc237 infected or mock-inoculated tg7 mice are shown. In panel (B), the electrophoretic pattern of proteinase K-treated tg7-rPrPHa PrP^{Sc} is shown as control (labeled +PK). MM, molecular mass markers. The western blots shown are representative of three independent experiments, and $n = 2$ mouse brains analyzed per passage.

the globular domain in the PrP N terminus is dispensable to the PrP^{Sc} infectious core.

The species barrier primarily dictates rPrP assemblies transmission efficacy

The systematic characterization of the transmission properties, biochemical and histomolecular features of hamster, human and mouse rPrP assemblies over four passages in hamster PrP transgenic mice unequivocally demonstrated their pathogenicity and the encoding of three different synthetic strains in their structure. Their adaptation process paralleled that seen with naturally occurring or laboratory prions with respect to the transmission/species barrier effect.

In the homotypic PrP transmission context with $rPrP^{Ha}$ assemblies, the 100% attack rate on first passage coupled with a $< 15\%$ shortening of the mean disease duration, and the stability of both the PrP^{res} signature and the clinical and neuropathological phenotype over subsequent passage suggested optimized propagation with minimal adaptation. The relative invariance of the disease duration observed over passaging is pivotal: (a) assessing reductions in disease duration from primary to secondary passage is a common strategy to unveil a species/transmission barrier [37,72–74], where a higher reduction signifies a stronger transmission barrier; (b) in the absence of a species barrier, a notable reduction may also indicate a low prion titer in the infecting inoculum at the primary passage. Figure 11A plots the disease duration ratio between the 1st and 2nd passage for various animal prions transmissions performed in our laboratory with tg7 mice (details in Table S3). It demonstrates that $rPrP^{Ha}$ assemblies behave like hamster-adapted laboratory scrapie strains, with straight propagation in tg7mice. The extended disease duration observed in tg7-$rPrP^{Ha}$ mice (~ 240 days at passage 4) compared to

17424658, 2024, 22, Downloaded from https://febs.onlinelibrary.wiley.com/doi/10.1111/febs.17291 by Université de Versailles-Saint-Quentin-en-Yvelines, Wiley Online Library on [22/05/2025]. See the Terms and Conditions (https://onlinelibrary.wiley.com/terms-and-conditions) on Wiley Online Library for rules of use; OA articles are governed by the applicable Creative Commons License

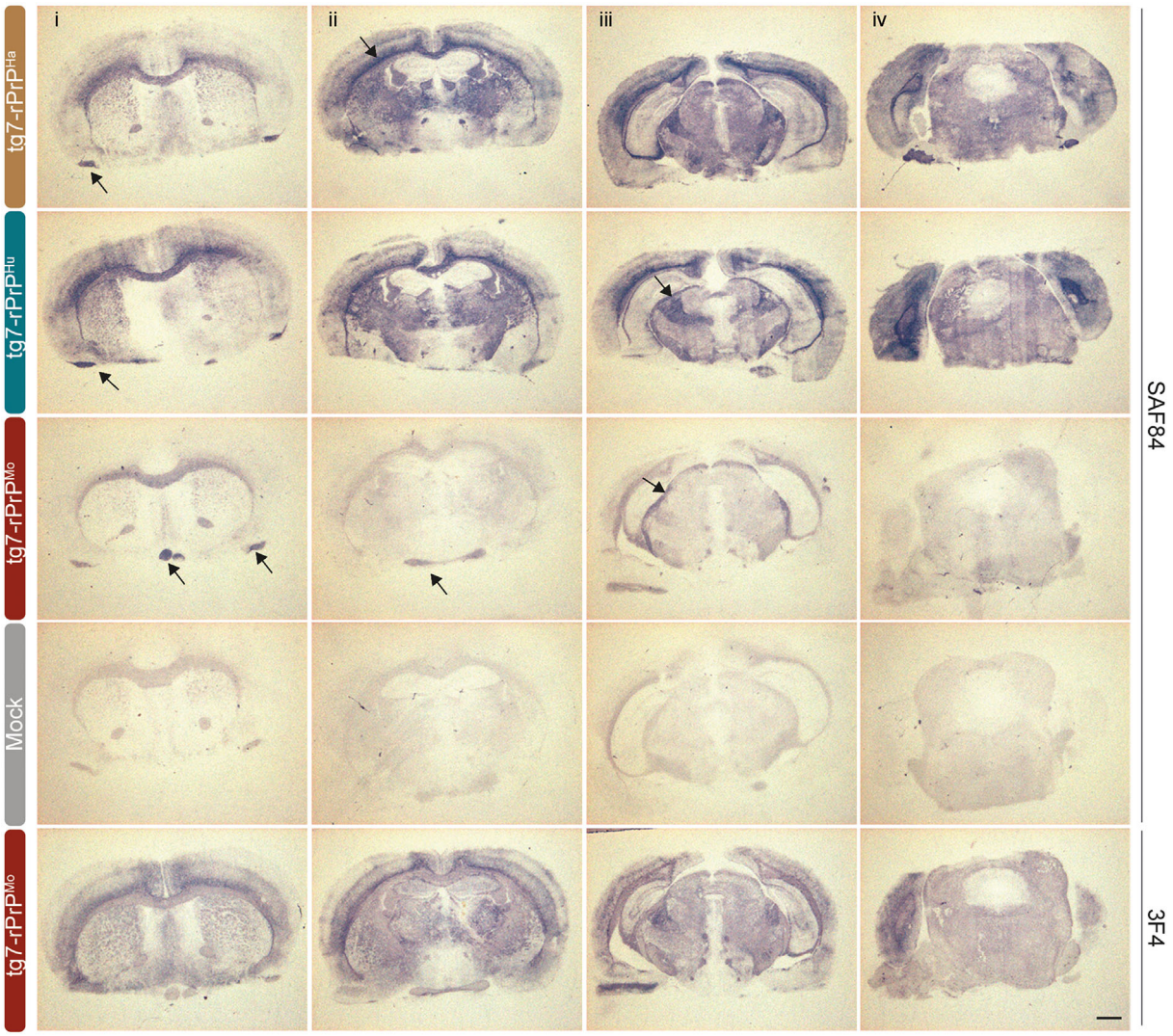

Fig. 7. Neuropathological pattern of PrP^{res} deposition in tg7 mice inoculated with recombinant PrP assemblies at the fourth passage. Representative histoblots of rostro-caudal transversal brain sections. Analyses were performed at the level of the septum (i), hippocampus (ii), midbrain (iii) and brainstem (iv) on $n = 3$ brains. As control, histoblots from mock-infected tg7 brain are shown. Histoblots were probed with SAF84 and 3F4 anti-PrP monoclonal antibodies to detect LMW PrP^{res} and HMW^{Mo} PrP^{res}, respectively (note that the levels HMW^{Hu} PrP^{res} were too low to be detected by histoblotting with 3F4). Arrows indicate PrP^{res} deposition in white matter tracts. Scale bar, 1 mm.

hamster-adapted prions (~40 to ~150 days; Fig. 11A) might be misconstrued as a less efficient disease process. However, it is crucial to consider prion titer and disease duration thoughtfully since the latter is intricately tied to prion toxicity [75]. In instances where prions exhibit high infectivity but low toxicity, the disease duration may be prolonged (variant and sporadic CJD prions have 'long' and 'short' disease durations in humanized mice, despite similar infectious titers [32,76]). Directly supporting the high prion titer of tg7-$rPrP^{Ha}$ synthetic prions, RT-QuIC experiments revealed seeding activity in the range of that from tg7-263K over the four passages. Therefore, we attribute the relatively prolonged disease duration to the unique characteristics of the tg7-$rPrP^{Ha}$ synthetic strain. The endogenous trimming of tg7-$rPrP^{Ha}$ PrP^{Sc} may influence its neurotoxic potential [64] or induce distinct neuronal dysfunction compared to full-length PrP^{Sc}.

In the heterotypic transmission context, $rPrP^{Bo}$ assemblies were not transmissible to tg7 mice, despite robust levels of seeding activity. This outcome was similar to that seen with naturally occurring bovine prions responsible for classical BSE or atypical H-BSE in these mice (Fig. 11B,C). In contrast, $rPrP^{Mo}$ and

17424658, 2024, 22, Downloaded from https://febs.onlinelibrary.wiley.com/doi/10.1111/febs.17291 by Université de Versailles-Saint-Quentin-en-Yvelines, Wiley Online Library on [22/05/2025]. See the Terms and Conditions (https://onlinelibrary.wiley.com/terms-and-conditions) on Wiley Online Library for rules of use; OA articles are governed by the applicable Creative Commons License

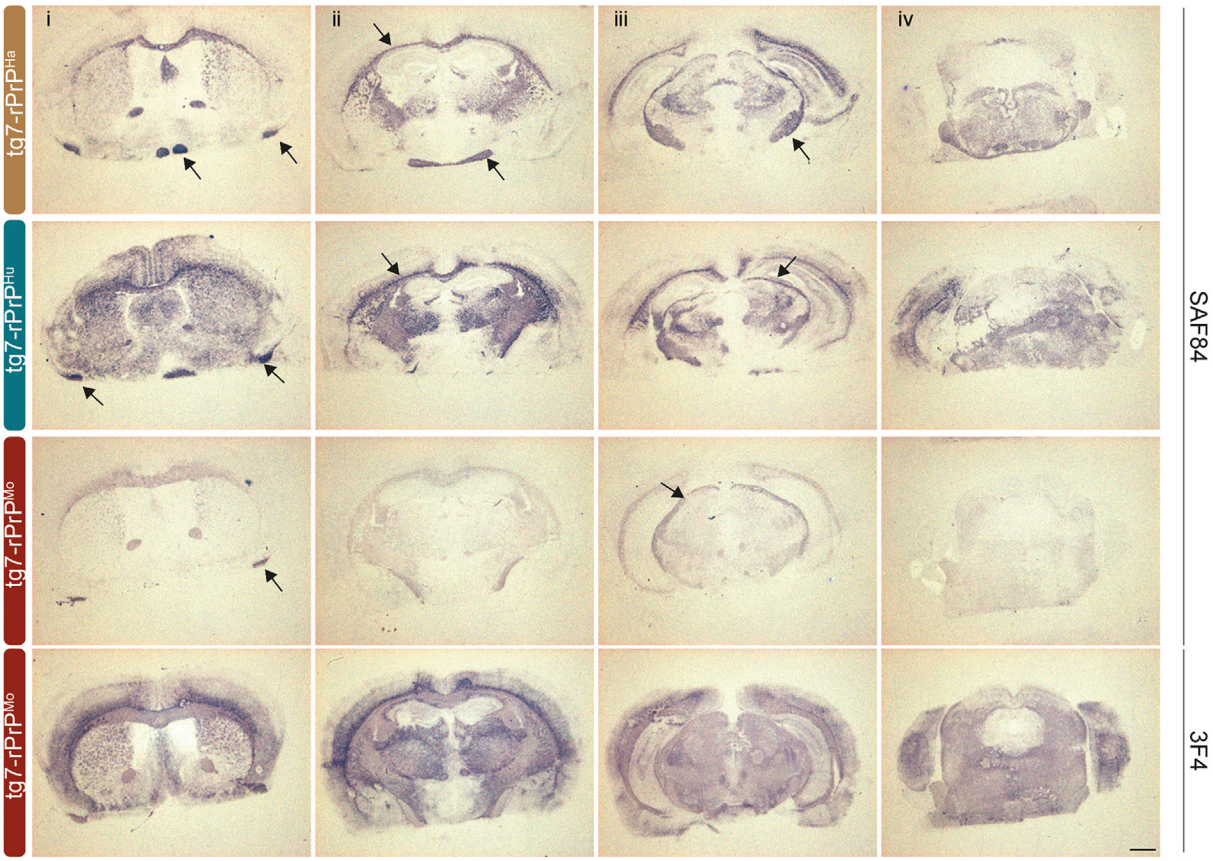

Fig. 8. Neuropathological pattern of PrP^{res} deposition in tg7 mice inoculated with recombinant PrP assemblies at the third passage. Representative histoblots of rostro-caudal transversal brain sections are shown at the 3rd passage, after challenge with recombinant PrP assemblies from hamster, human and mouse species. Analyses were performed at the level of the septum (i), hippocampus (ii), midbrain (iii) and brainstem (iv) on $n = 3$ brains. Histoblots were probed with 3F4 and SAF84 anti-PrP monoclonal antibody, as indicated. Arrows indicate PrP^{res} deposition in white matter tracts. Scale bar, 1 mm.

rPrP^{Hu} assemblies induced clinical disease at a complete or near-complete attack rate. The disease evolution differed from that observed with rPrP^{Ha} on subpassaging. The disease durations evolved markedly, either abruptly becoming very short with rPrP^{Mo} assemblies or decreasing more slowly with rPrP^{Hu} assemblies. There was no drastic change in seeding activity over passaging, suggesting that the significant reduction in incubation times truly reflects and adaptation process, not a gain of activity. Notably, the disease ratio between the 1st and 2nd passages for rPrP^{Mo} was among the highest observed in tg7 mice, similar to that seen with atypical L-BSE prions (Fig. 11A), which also underwent abrupt evolution on subpassage (Fig. 11D). The transmission properties of rPrP^{Mo} and rPrP^{Hu} assemblies thus mirrored those observed in the evolution of naturally occurring prions in the context of a species barrier or a transmission barrier, involving gradual or rather abrupt ('mutational') adaptation to optimized pathogenesis [27,28,37,73,74,77].

In tg7-rPrP^{Mo} synthetic prions, a mixture of LMW and HMW^{Mo} PrP^{Sc} was consistently observed in western blot migration profiles across passages, indicating that the degree of adaptation to the new hamster PrP sequence did not significantly alter this pattern. Conversely, in tg7-rPrP^{Hu} brains, only LMW PrP^{res} was detected over three passages before HMW^{Hu} PrP^{res} species emerged, and this transition did not significantly impact the disease duration. This decoupling of the appearance of 'classical' PrP^{res} profile and adaptation contrasts with the 'deformed-templating' hypothesis ([38] and the Introduction). Instead, it supports the notion that our rPrP-derived prions undergo conformational diversification similar to naturally occurring prions (for review [3]).

Overall, we observed that rPrP assemblies behave similarly to naturally occurring prions, with PrP sequence

17424658, 2024, 22, Downloaded from https://febs.onlinelibrary.wiley.com/doi/10.1111/febs.17291 by Université de Versailles-Saint-Quentin-en-Yvelines, Wiley Online Library on [22/05/2025]. See the Terms and Conditions (https://onlinelibrary.wiley.com/terms-and-conditions) on Wiley Online Library for rules of use; OA articles are governed by the applicable Creative Commons License

mismatches and strain types influencing the force of prion species/transmission barriers. This suggests that the PrP backbone alone, without post-translational modifications or co-factors, allows sufficient structural remodeling during the misfolding process to encode different strains and phenotypic properties, including cross-species transmission capacities.

Using hamster PrP transgenic mice instead of hamsters for the bioassay is not a limitation in our study. There is compelling evidence that transgenic animals that overexpress PrP are highly relevant reporter models for comparing prion strain properties and cross-species transmission capacities and have a greater chance of success than wild-type animals (for reviews [24–26]), due to acceleration of disease development, when it occurs (Fig. 11 for tg7 mice and [56,78–80] for other transgenic models). In addition, using hamster brain homogenate in our PMCA experiments as source of PrP^{C} provides clear evidence that tg7 mice do not aberrantly react compared to hamsters to amplify tg7-rPrP synthetic prions. They also lend support to the view that hamsters would replicate these prions.

An infectious C-terminal PrP^{Sc} fragment

The LMW PrP^{res} pattern identified in the three synthetic prion strains consists of 2 N-terminally truncated fragments that start around amino acids ~140–145 and 150–155. The use of thermolysin as chemical probe and differential centrifugation further indicated that these truncations primarily occur *in vivo*. This implies that PrP^{Sc} is internalized and undergoes endocytic processes during replication in the brain. However, the association of extensive vacuolation (Fig. 9) with intraneural PrP^{Sc} raises some controversy compared to naturally occurring prions [81]. It also prompts questions about the respective contributions to neurodegeneration of these conformations versus classical PrP^{Sc} when both are co-propagated in the brain of rPrP-tg7 mice. The same questions remain valid for naturally occurring prions, be there of animal or human origin, as variably glycosylated PrP^{res} fragments with a C-terminal core similar or slightly shorter than LMW PrP^{res} have been identified in the brain of patients with sporadic CJD, in the brain of cattle with atypical H-type BSE and in ovine PrP mice inoculated with certain sheep scrapie isolates [82–84].

Recently, we demonstrated that alpha-cleaved C1-fragments from PrP^{C} (truncation at amino acids 113/115, [85]) were convertible into prions in RK13 cells, when part of the α-helix H2 was deleted [86]. This result, along with the infectivity of LMW PrP^{Sc} fragments found here, appears to contradict several reports suggesting that PrP amino acids ~90–100 to 155, notably the central polybasic domain with four lysines at amino acids ~100–110, are an obligate domain of the PrP^{res} infectious core [40,48,87–90]. This indicates that the fold allowing prion infectivity and the strain structural determinant can undergo significant variations with respect to the PrP domains involved.

Recombinant PrP assemblies heterogeneity may facilitate heterotypic transmission

Why can our rPrP assemblies preparations adapt or not in a heterotypic PrP context? In previous reports, we detailed the intrinsic generation of two sets of infectious/replicative PrP^{Sc} assemblies during the early steps of prion conversion: a small oligomeric species smaller than a pentamer and a larger species exceeding a MDa in size. These two species influence their own formation through kinetical feedback [22]. We proposed that their synergetic interaction is essential for prion adaptation and overcoming species barriers [37]. Mechanistically, we hypothesized that this interaction, either directly or through their elementary subunits [58], creates a templating interface for heterotypic PrP^{C} that is topologically absent in each subtype taken independently. The spherical and fibrillar objects in the rPrP assemblies may similarly interact, as suggested by AFM images, and favor conversion in the heterotypic PrP context. While many reasons could explain why the bovine rPrP assemblies were unable to propagate in tg7 mice, it is noteworthy that such structural heterogeneity was not observed in these preparations.

Previous studies on synthetic prions used fibrillar preparations purified to structural homogeneity [38] or employed preparations generated by *in vitro* self-amplification in the potential presence of different co-factors. This practice may have selected certain assemblies and/or modified the relative ratio of conformations [22], resulting in delayed or inefficient transmission. In the realm of soft matter biochemistry and amyloid structural biology, tuning physico-chemical conditions to achieve a high degree of structural homogeneity is a common practice.

Are LMW prions compatible with recent prion PIRIBS architectures?

Recent cryo-EM studies of purified PrP^{res} from hamster 263K, and mouse RML or ME7 prion strains—with PK-resistant cores spanning ~90 to ~230—revealed a common structure. This structure is characterized by a single- or paired-protofilament helical structure with a PIRIBS-based core architecture

17424658, 2024, 22, Downloaded from https://febs.onlinelibrary.wiley.com/doi/10.1111/febs.17291 by Université de Versailles-Saint-Quentin-en-Yvelines, Wiley Online Library on [22/05/2025]. See the Terms and Conditions (https://onlinelibrary.wiley.com/terms-and-conditions) on Wiley Online Library for rules of use; OA articles are governed by the applicable Creative Commons License

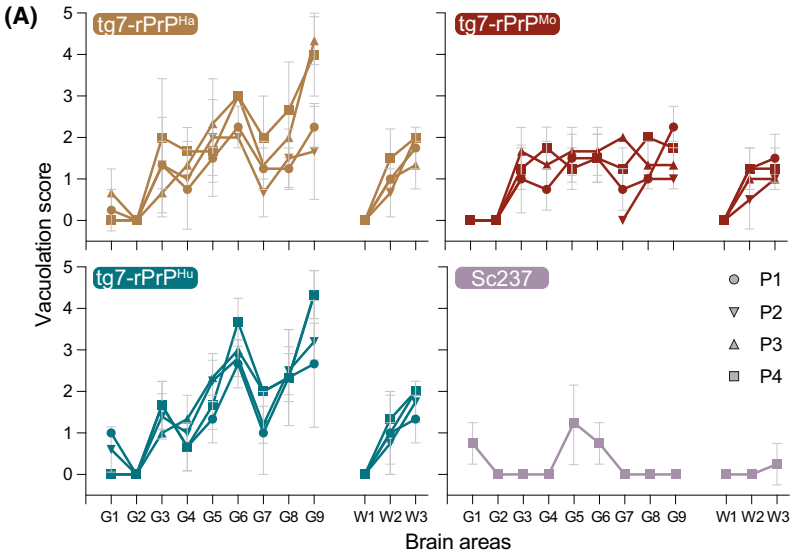

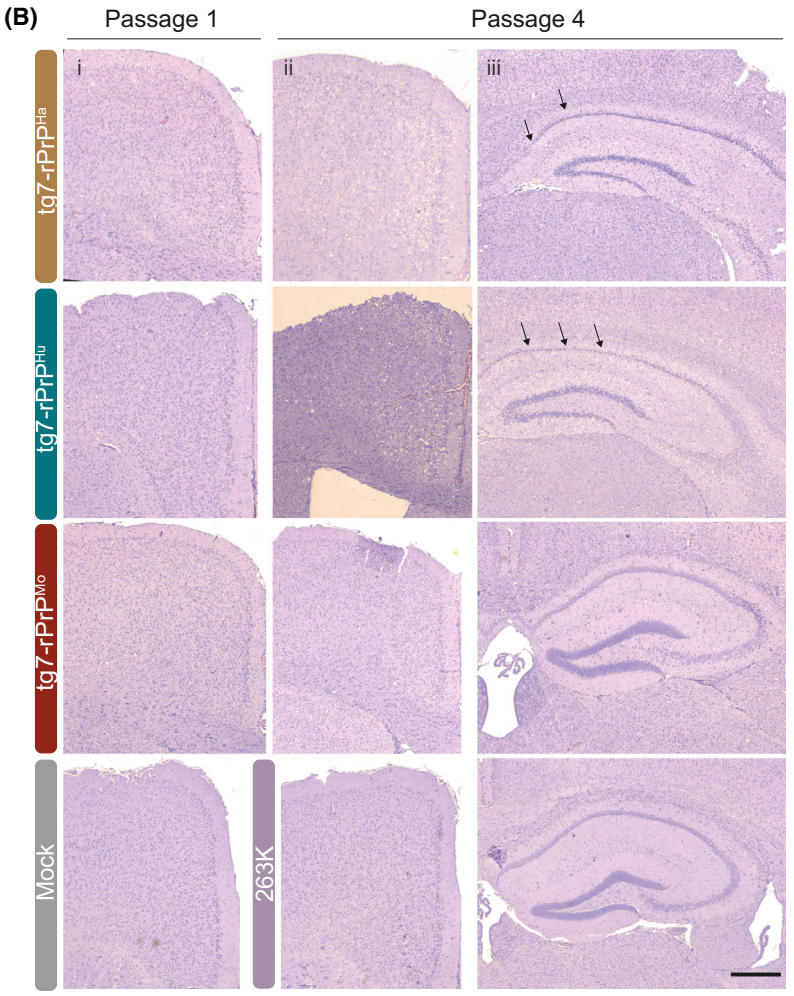

The FEBS Journal **291** (2024) 5051–5076 © 2024 The Author(s). *The FEBS Journal* published by John Wiley & Sons Ltd on behalf of Federation of European Biochemical Societies.

17424658, 2024, 22, Downloaded from https://febs.onlinelibrary.wiley.com/doi/10.1111/febs.17291 by Université de Versailles-Saint-Quentin-en-Yvelines, Wiley Online Library on [22/05/2025]. See the Terms and Conditions (https://onlinelibrary.wiley.com/terms-and-conditions) on Wiley Online Library for rules of use; OA articles are governed by the applicable Creative Commons License

Fig. 9. Spongiform degeneration in the brains of mice infected with recombinant PrP-derived synthetic prions. (A) Standard vacuolar lesion profiles at passage (P) 1 to 4. Sc237 in tg7 mice was used as control. The vacuolation intensity was scored as means ± SD in standard gray (G1–G9) and white (W1–W3) matter areas. G1: dorsal medulla; G2: cerebellar cortex; G3: superior colliculus; G4: hypothalamus; G5: medial thalamus; G6: hippocampus; G7: septum; G8: medial cerebral cortex at the level of the thalamus; G9: medial cerebral cortex at the level of the septum; W1: cerebellar white matter; W2: white matter of the mesencephalic tegmentum; and W3: pyramidal tract. Tg7-rPrP^{Mo} at 2nd passage was not complete because brains deteriorated. $n = 3$ (passage 3 and 4) to $n = 5$ (passage 1 and 2) brains were used to establish the profiles. (B) Fixed sections stained with hematoxylin and eosin show the cingulate cortex (i, ii) and hippocampus (iii) where spongiosis was prominent at passage 1 and 4. Note the severe neuronal degeneration in the pyramidal cell layer of the hippocampus with tg7rPrP^{Ha} and tg7-rPrP^{Hu} prions (arrows). Scale bar: 400 μm.

[12–14]. Applying the hamster 263K-PIRIBS architecture to hamster LMW PrP^{res} would remove ~35% of the β-strands in the N terminus lobe and structural elements proximal to the C-terminal flank, potentially affecting overall stability. However, cryo-EM analyses of misfolded assemblies of recombinant PrP molecules from different species and with different truncations or mutations showed a global conservation of the PIRIBS architecture. Different PrP domains can form the ordered fibrillar core [4]. Specifically, the C-terminal region spanning positions ~170 to ~230 could form a PIRIBS motif. Further stability may also be provided by an organization in two closely packed symmetrical protofilaments [91]. Studying LMW PrP^{Sc} architecture by Cryo-EM will be of upmost interest.

In summary, our study demonstrates that 'pure' rPrP assemblies possess full pathogenicity, and the synthetic prions generated exhibit an inherent ability to diversify and adapt in the presence of a species barrier. Preliminary findings indicate that transmission of rPrP assemblies to an intermediate host PrP species modifies the strain spectrum and capacity to adapt on backpassage to tg7 mice, further highlighting that their evolutive potential mirrors that of naturally occurring prions.

Materials and methods

Biosafety

The formation of rPrP assemblies, prion protein biochemistry, mouse experimentation and histopathology were conducted in biosafety level 2 or level 3 facilities, strictly following safety protocols. AFM analyses were performed in a biosafety level 1 laboratory using dedicated sample holders and equipment, in accordance with approved biosafety procedures. All safety protocols were reviewed and approved by Local and National Prion Research Committees.

Formation of recombinant PrP fibrillar assemblies

Full-length rPrP with amino acid sequence corresponding to hamster, human (M_{129} allele), mouse, bovine (6 copies of the octapeptide repeat sequence) were produced in *Escherichia coli* and purified as previously described [92]. The purified, monomeric forms of rPrP were lyophilized and stored. The conversion of the monomers into amyloid-like assemblies was performed as previously described (Fig. S1, [93,94]). Briefly, lyophilized proteins were dissolved directly in 50 mM MES buffer, pH 6.0 (1 mg·mL^{-1} final concentration), kept on ice, and used to prepare a 600 μL reaction. The reaction mixture, consisting of water (90 μL), guanidine hydrochloride (6 M, 200 μL), MES buffer (0.5 M, pH 6.0, 10 μL) and PrP stock solution (300 μL), was incubated with continuous orbital shaking at 30 r.p.m. (16 mm amplitude) at 37 °C. Fibril formation was monitored using a thioflavin T binding assay [92]. Aliquots were diluted into a 10 mM sodium acetate buffer, pH 5.0, to a final PrP concentration of 0.3 μM, and thioflavin T was added to a final concentration of 10 μM. Samples were then dialyzed in 10 mM sodium acetate, pH 5.0. Fibrils were collected by ultracentrifugation for 45 min at 228 147 ***g*** using a Beckman Optima TL100 ultracentrifuge and a TLA-100.3 rotor, and resuspended in 10 mM sodium acetate, pH 5.0. A washing step was performed by repeating the ultracentrifugation and resuspension steps. All concentrations given for fibrillar PrP refer to the respective equivalent monomer concentration. The oligomers were isolated from 1-week-old assemblies by 1-h ultracentrifugation at 228 147 ***g*** at 4 °C. Most of the fibrils sedimented, while small oligomeric objects, including spherical objects, remained in the supernatant.

Atomic force microscopy and dynamic light scattering

AFM experiments were performed on a NanoWizard 3 (JPK, Berlin, Germany) in liquid, using a nanoprobe of 10 Å diameter (Peakforce-HIRS-F-B2) in a liquid bio-cell chamber in QI mode. Recombinant PrP assemblies at a concentration of 0.5 μM equivalent monomer were deposited on a freshly cleaved mica surface for 3 min. After two iteratives washes of the mica surface with sodium acetate buffer (10 mM, pH5.0), the bio-cell compartment was filled with 1 mL buffer. The size of different types of assemblies was estimated using a combination of JPK image analysis interface and a homemade MATLAB code. The mean average hydrodynamic size of the assemblies was determined by

17424658, 2024, 22, Downloaded from https://febs.onlinelibrary.wiley.com/doi/10.1111/febs.17291 by Université de Versailles-Saint-Quentin-en-Yvelines, Wiley Online Library on [22/05/2025]. See the Terms and Conditions (https://onlinelibrary.wiley.com/terms-and-conditions) on Wiley Online Library for rules of use; OA articles are governed by the applicable Creative Commons License

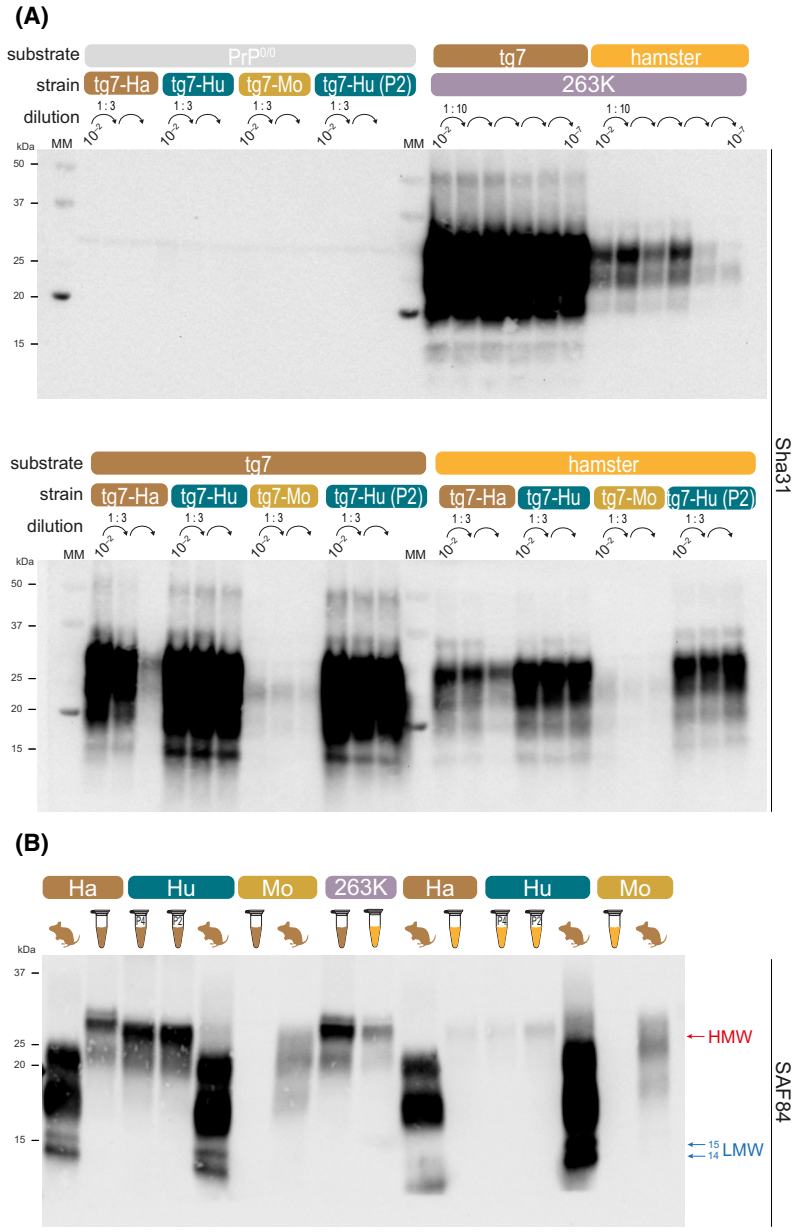

Fig. 10. Amplification of recombinant PrP-derived synthetic prions by protein misfolding cyclic amplification assay (PMCA). (A) Serial 1 : 3 dilutions of brain samples from tg7-rPrP^{Ha}, tg7-rPrP^{Hu} and tg7-rPrP^{Mo} mice at passage 4 (Ha, Hu, Mo) or 2 (Hu (P2)) were submitted to 4 rounds of PMCA using brain lysates from PrP$^{0/0}$ mice, tg7 mice or hamsters, as substrates. As positive control, 1 : 10 dilutions of brain samples from tg7-263K mice were used. Aliquots of the PMCA products were digested with proteinase K and analyzed by immunoblot using Sha31 antibody (representative immunoblot of $n = 3$ independent PMCA experiments). (B) Comparison of the PrP^{res} patterns after PMCA amplification (symbolized by a tube) using tg7 (brown) or hamster (yellow) brain lysates or by transmission to tg7 mice (symbolized by a mouse) using SAF 84 antibody which preferentially detects LMW PrP^{res}. MM: molecular mass markers. The immunoblot shown is representative of $n = 3$ electrophoretic analyses.

dynamic light scattering. The number of spherical objects per μm^2 was estimated using a homemade MATLAB script. The statistics were performed by estimating the number of spherical objects on four different AFM fields of 500 × 500 nm. The data were then normalized to 1 μm^2.

Animal experiments

Animal experiments adhered strictly to European Union directive 2010/63 guidelines and received approval from the INRAE Local Ethics Committee (Comethea; permit numbers 12-034, 15-056 and APAFIS#29603-20210209145252 15). They were performed in accordance with the Animal Research: Reporting of *In Vivo* Experiments (ARRIVE) 2.0 guidelines. The hamster PrP tg7 line, described previously [15,55,56], was employed. It was kindly provided by CSL-Behring (Marburg, Germany) and originates from S. Prusiner laboratory [95]. This line, homozygous for the hamster PrP transgene, was established on the Zurich I PrP$^{0/0}$ mouse background. Level of overexpression is ~4-fold compared to golden Syrian hamster brain (Fig. 1B,C). These mice, showing no abnormal phenotype or neurological signs with aging, have a normal life span of around 1.5–2 years and do not develop spontaneous prion disease

17424658, 2024, 22, Downloaded from https://febs.onlinelibrary.wiley.com/doi/10.1111/febs.17291 by Université de Versailles-Saint-Quentin-en-Yvelines, Wiley Online Library on [22/05/2025]. See the Terms and Conditions (https://onlinelibrary.wiley.com/terms-and-conditions) on Wiley Online Library for rules of use; OA articles are governed by the applicable Creative Commons License

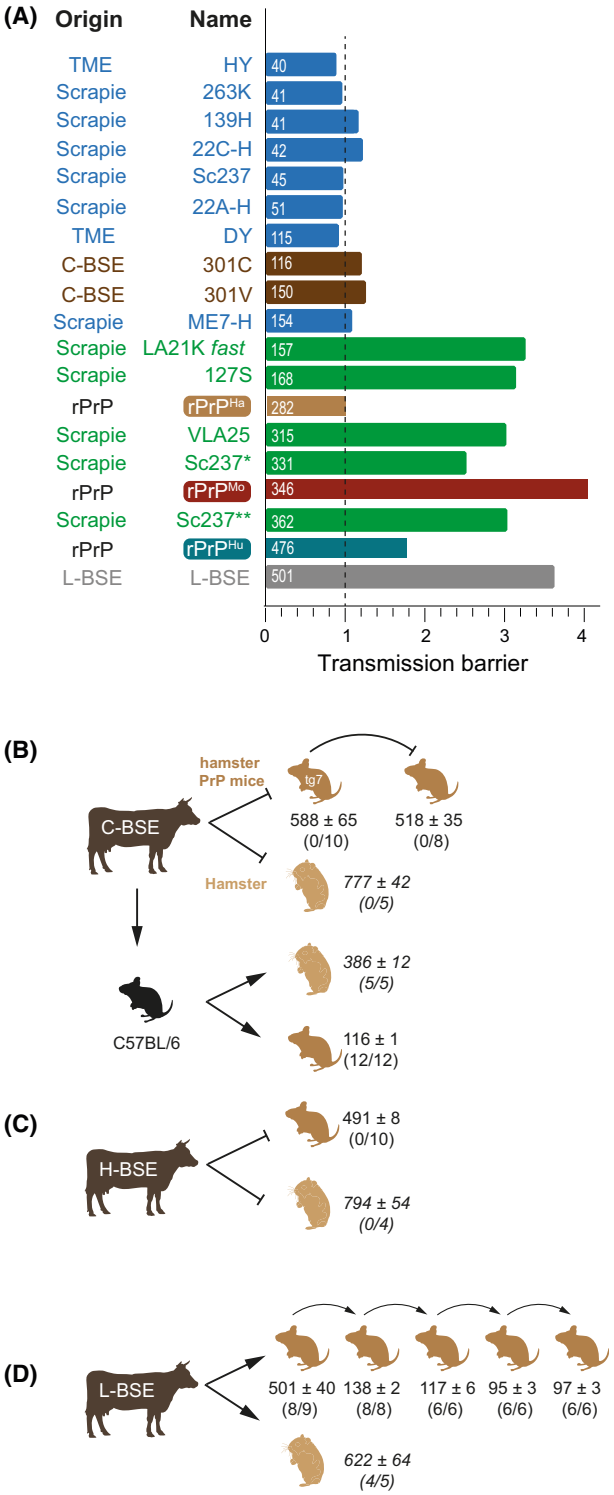

Fig. 11. Magnitude of the transmission barrier of recombinant PrP assemblies versus that of animal prions following transmission to tg7 mice. (A) Graph showing the magnitude of the transmission barrier. It is calculated as the ratio of the mean incubation durations on first to second passage [37,72]. A value of 1 (dash line) indicates absence of transmission barrier. The magnitude of the transmission barrier observed with the recombinant PrP assemblies is compared to that of animal prions (sheep scrapie, classical form bovine spongiform encephalopathy (C-BSE), transmissible mink encephalopathy (TME)) experimentally adapted or passaged in Syrian hamsters (blue), mouse (brown), and tg338 transgenic mice expressing ovine PrP (green) before inoculation to tg7 mice. (*) and (**) indicate that spleen material at third and fourth passage of Sc237 in tg338 mice was used (raw transmission data in Table S3). L-type BSE directly originates from cattle (see below). The mean incubation times on primary passage are indicated in white color. (B–D) Summary of transmissions of BSE prions to tg7 mice. Classical BSE prions (C-BSE strain) and atypical BSE prions (H-BSE and L-BSE strains) were inoculated by intracranial route to tg7 transgenic mice expressing hamster PrP (10% w/v concentration, same inoculation protocol as described in the Materials and methods section or previously [28,102,103]). The transmission properties of these BSE isolates, including in heterotypic PrP contexts, have been previously published ([28,102,103], C-BSE isolate is BSE Fr3; H-BSE isolate is Fr2; L-BSE isolate is It1088). Only L-BSE prions were directly pathogenic in tg7 mice. C-BSE prions were pathogenic in tg7 mice after serial passage and adaptation in C57BL/6 mice (301C mouse-BSE strain [104]). For comparison, the transmission properties of the same BSE prion strains in golden Syrian hamsters (*Mesocricetus auratus*) are shown (data in italics from [105]). The outcomes at first passage were similar, indicating that the force of the species barrier for atypical, classical and mouse-adapted BSE prions is equivalent between transgenic mice overexpressing hamster PrP and hamsters. For each set of transmission, the mean survival times ± SEM (in days) are indicated. The number of disease and/or PrP^{Sc}-positive animals/number of inoculated animals are in bracket.

upon intracerebral inoculation with uninfected brain material ($n = 450$ mice inoculated and followed over 600 days in our laboratory). Only tg7 females aged 6–8 weeks at the time of inoculation were used. Mice were group-housed by 4 to 5 in polypropylene cages in a standard temperature- and humidity-controlled biosafety laboratory 3 animal facility, with a 12-h light–dark rhythm, unlimited access to food and water, and provided enrichment items (igloos, wood toys, nests). Cages, food, enrichment, and water were sterilized before use.

Mouse bioassays

The methodology used has been described previously [96]. To prevent cross-contamination, a strict protocol using disposable equipment and preparation of all inocula in a class II microbiological cabinet was followed. Recombinant PrP assemblies and monomers were extemporaneously prepared at a concentration of 0.5 $mg{\cdot}mL^{-1}$ in 5% w/v glucose. Individually identified tg7 mice (8–10 mice per group) were intracerebrally inoculated with 20 µL of the solution, using a 27-gauge disposable syringe needle inserted into the right

17424658, 2024, 22, Downloaded from https://febs.onlinelibrary.wiley.com/doi/10.1111/febs.17291 by Université de Versailles-Saint-Quentin-en-Yvelines, Wiley Online Library on [22/05/2025]. See the Terms and Conditions (https://onlinelibrary.wiley.com/terms-and-conditions) on Wiley Online Library for rules of use; OA articles are governed by the applicable Creative Commons License

parietal lobe. Animals were anesthetized with 3% isoflurane during the procedure and placed on a heating pad until they fully recovered. They were monitored daily for general health. Animals were euthanized at terminal stage or at end-life by cervical column dislocation. Brains were carefully collected with separate, disposable tools, homogenized at 20% w/v in 5% glucose and stored at −80 °C until further use. For subpassaging, 20 µL of the brain solution was intracerebrally inoculated at 10% w/v to individually identified tg7 mice (5–8 mice per group). At each passage, brains were also directly frozen on dry ice (for histoblotting) before storage at −80 °C or fixed by immersion in neutral-buffered 10% formalin (for lesion profiling).

Real-time-quacking induced conversion

RT-QuIC amplifications were performed as previously described [60,96,97]. Briefly, 1 µL of 10% brain homogenates or 1 µL of 20 µM rPrP assemblies underwent serial 10-fold dilutions in 20 mM sodium phosphate buffer pH 7.4, 130 mM NaCl, 0.1% SDS and 1× N2 supplement (ThermoFisher Scientific, Nalgene Nunc International, Villebon-sur-Yvette, France). Subsequently, 2 µL of each dilution was loaded into individual wells of a black 96-well optical bottom plate containing 98 µL of 20 mM sodium phosphate buffer pH 7.4, 300 mM NaCl, 10 µM thioflavin T, 1 mM EDTA and 100 $\mu g \cdot mL^{-1}$ of either purified recombinant wild-type human PrP (Met_{129} allele) or hamster PrP. The plate was sealed using Nunc Amplification Tape (ThermoFisher Scientific), placed in a Xenius XM spectrofluorometer (Safas, Monaco, Monaco) and incubated for 24–60 h at 46 °C ± 2 °C. Throughout the measurements, cycles of 1-min orbital shaking (600 r.p.m.) and 1-min rest were applied, and fluorescence was recorded every 30 min. Experiments were performed in quadruplicates. Each curve was fitted using the MATLAB software (R2022b, MathWorks, Meudon, France) with the equation: $I = I_{min} + \frac{(I_{max} - I_{min})X^n}{(K + X^n)}$, where I is the fluorescence intensity and X is the time. Seeding activity titer (SD_{50}; seeding dose giving thioflavin T positivity in 50% of the replicates) was estimated by the Spearman–Kärber method [98]. The values were expressed as SD_{50} per mL of 10% (w/v) brain homogenate or as SD_{50} per mL of 20 µM rPrP assemblies.

Protein misfolding cyclic amplification

PMCA was conducted according to an optimized in-house technology [57], using brain lysates (10% w/v) from tg7 mice, PrP knock-out mice (Zürich I line [99]) and from golden Syrian hamsters (René Janvier, Laval, France) as substrates, and serial 1 : 3 dilutions of tg7-$rPrP^{Ha}$, tg7-$rPrP^{Mo}$ (passage 4) and tg7-$rPrP^{Hu}$ (passages 2 and 4) prions or serial 1 : 10 dilutions of tg7-263K prions as seeds. The mixture was subjected to four rounds of 96 cycles of 30-s sonications (220–240 Watts) followed by 29.5 min of incubation at 37 °C. Between each round, the reaction products were diluted 1 : 3 with fresh substrate. PMCA was performed in a 96-well microplate format (Axygen, Corning, Boulogne-Billancourt, France) using a Qsonica-Misonix Q700 sonicator (Delta Labo, Colombelles, France). The amplified products were PK-digested (115 $\mu g \cdot mL^{-1}$ final concentration, 0.6% SDS, 1 h, 37 °C) before immunoblot analyses, as described below.

Analysis of PK-resistant PrP^{Sc} by immunoblot

PrP^{res} was extracted from 20% brain homogenates with the Bio-Rad TeSeE detection kit, as previously described [27,32]. In brief, 200 µL aliquots were digested with proteinase K (200 $\mu g \cdot mL^{-1}$ final concentration in buffer A) for 10 min at 37 °C, followed by before precipitation with buffer B and centrifugation at 28 000 ***g*** for 5 min. Pellets were then resuspended in Laemmli sample buffer, denatured, separated on 12% Bis-Tris Criterion gels (Bio-Rad, Marne la Vallée, France), electrotransferred onto nitrocellulose membranes, and probed with primary anti-PrP antibodies (list and epitopes in Table S2) and ad hoc secondary antibodies. Immunoreactivity was visualized using chemiluminescence (Pierce ECL, Thermo Scientific, Montigny le Bretonneux, France). Chemiluminescent signals were captured with the Chemidoc digital imager and analyzed using IMAGE LAB software (Bio-Rad). Enzymatic deglycosylation of denatured PrP^{res} was performed with 1000 U of recombinant PNGase (peptide *N*-glycosidase F; New England Biolabs, Evry, France) for 2 h at 37°C in 1% Nonidet P40 and the manufacturer's buffer.

Analysis of thermolysin-resistant PrP^{Sc} by immunoblot

Mouse brain homogenates were diluted in lysis buffer (2% sodium deoxycholate, 2% Triton X-100, 200 mM Tris–HCl pH7.4) containing thermolysin (final concentration 125 $\mu g \cdot mL^{-1}$) and incubated for 1 h at 70 °C under constant agitation at 800 r.p.m. The samples were analyzed by immunoblot, as above.

PrP^{Sc} insolubility assay

The entire procedure was performed at 4 °C. Aliquots (6 µL) of tg7-brain homogenates were mixed with a protease inhibitor mixture (Roche, Mannheim, Germany) and 5% glucose (94 µL). An equal volume of solubilization buffer (50 mM HEPES pH 7.4, 300 mM NaCl, 10 mM EDTA, 4% w/v dodecyl-β-D-maltoside) was added, followed by a 45-min incubation. Sarkosyl (*N*-lauryl sarcosine; Sigma Aldrich, Saint-Quentin-Fallavier, France) was then added to a final concentration of 2% w/v, and the incubation continued for a further 45 min [15]. The mixture was then loaded on a 40% w/v sucrose gradient before

17424658, 2024, 22, Downloaded from https://febs.onlinelibrary.wiley.com/doi/10.1111/febs.17291 by Université de Versailles-Saint-Quentin-en-Yvelines, Wiley Online Library on [22/05/2025]. See the Terms and Conditions (https://onlinelibrary.wiley.com/terms-and-conditions) on Wiley Online Library for rules of use; OA articles are governed by the applicable Creative Commons License

centrifugation at 100 000 ***g*** for 1 h at 4 °C, using a Beckman Optima TL100 ultracentrifuge. This resulted in supernatant and pellet fractions, with proteins in the pellet resuspended in Laemmli sample buffer, denatured and analyzed by immunoblot, as described above.

Histoblots

Brain cryosections were cut at 8–10 µm (NX-70, MM, Lyon, France), transferred onto Superfrost slides and stored at −20 °C until use. Histoblot analyses, using the 3F4 or SAF84 anti-PrP antibodies (Table S2), were performed on 2–3 brains per passage [32]. Image acquisition was performed with a digital camera (Coolsnap, Photometrics, Paris, France) mounted on a binocular glass (SZX12, Olympus, Paris, France).

Vacuolar lesion profiles

Hematoxylin-eosin-stained paraffin-embedded brain tissue sections were used to establish standardized vacuolar lesion profiles in mice, as previously described [100,101]. Analyses were performed on 3–5 brains per passage.

Statistical analysis

The GRAPHPAD PRISM 9.0 software (GraphPad, La Jolla, CA, USA) was used to establish the Kaplan–Meier curves plotting the percentage of mice without prion disease against the incubation time. This software was also used to draw the RT-QuiC curves and the vacuolation profiles.

Terminology

The term rPrP refers to recombinant PrP (monomers and assemblies) with the mammalian species of origin in superscript (Ha, hamster; Hu, human; Mo, mouse; Bo, bovine). The term tg7-rPrP refers to synthetic prions derived from the inoculation of rPrP assemblies to tg7 mice, with the species of origin indicated in superscript. Due to space constraint in the figures, sometimes the term tg7-species is used.

Acknowledgements

We thank the staff of Animalerie Rongeurs (INRAE, Infectiology of fishes and rodent facility, doi: 10.15454/1.5572427140471238E12, Jouy-en-Josas, France) for animal care. We thank Byron Caughey (NIH, RML, Montana, USA), Jan Langeveld (Wageniggen University, NL) and Stéphanie Simon (CEA Saclay, France) for providing us with R20, 12B2 and SAF34 antibodies, respectively. This work was supported by grants from the Agence Nationale de Sécurité du Médicament et des Produits de Santé, France (Starting grant, 2014S033 HAP ANSM 2014/iPDB), from the Fondation pour la Recherche Médicale, France (Equipe FRM DEQ20150331689), from the European Research Council (ERC Starting Grant SKIPPERAD, number 306321) and from the French National Research Agency (ANR21-CE-15-0011 PrionDif).

Conflict of interest

The authors declare no conflict of interest.

Author contributions

VB and HR designed research. HR, DM, LH, FR, AMM, MM, NA, AI, HK, SY, J-BM, PS, OA, JT and VB performed research and analyzed data. VB and HR wrote the paper.

Peer review

The peer review history for this article is available at https://www.webofscience.com/api/gateway/wos/peer-review/10.1111/febs.17291.

Data availability statement

The data that support the findings of this study are available in the Materials and methods and/or Supporting Information of this article.

References

1 Riek R, Hornemann S, Wider G, Billeter M, Glockshuber R & Wuthrich K (1996) NMR structure of the mouse prion protein domain PrP(121-231). *Nature* **382**, 180–182.
2 Eghiaian F, Grosclaude J, Lesceu S, Debey P, Doublet B, Treguer E, Rezaei H & Knossow M (2004) Insight into the PrPC → PrPScconversion from the structures of antibody-bound ovine prion scrapie-susceptibility variants. *Proc Natl Acad Sci U S A* **101**, 10254–10259.
3 Igel A, Fornara B, Rezaei H & Beringue V (2022) Prion assemblies: structural heterogeneity, mechanisms of formation, and role in species barrier. *Cell Tissue Res* **392**, 149–166.
4 Artikis E, Kraus A & Caughey B (2022) Structural biology of ex vivo mammalian prions. *J Biol Chem* **298**, 102181.
5 Manka SW, Wenborn A, Collinge J & Wadsworth JDF (2023) Prion strains viewed through the lens of cryo-EM. *Cell Tissue Res* **392**, 167–178.
6 Collinge J (2001) Prion diseases of humans and animals: their causes and molecular basis. *Annu Rev Neurosci* **24**, 519–550.

17424658, 2024, 22, Downloaded from https://febs.onlinelibrary.wiley.com/doi/10.1111/febs.17291 by Université de Versailles-Saint-Quentin-en-Yvelines, Wiley Online Library on [22/05/2025]. See the Terms and Conditions (https://onlinelibrary.wiley.com/terms-and-conditions) on Wiley Online Library for rules of use; OA articles are governed by the applicable Creative Commons License

7 Fernandez-Borges N, Parra B, Vidal E, Erana H, Sanchez-Martin MA, de Castro J, Elezgarai SR, Pumarola M, Mayoral T & Castilla J (2017) Unraveling the key to the resistance of canids to prion diseases. *PLoS Pathog* **13**, e1006716.

8 Bian J, Khaychuk V, Angers RC, Fernandez-Borges N, Vidal E, Meyerett-Reid C, Kim S, Calvi CL, Bartz JC, Hoover EA *et al.* (2017) Prion replication without host adaptation during interspecies transmissions. *Proc Natl Acad Sci U S A* **114**, 1141–1146.

9 Sarradin P, Viglietta C, Limouzin C, Andreoletti O, Daniel-Carlier N, Barc C, Leroux-Coyau M, Berthon P, Chapuis J, Rossignol C *et al.* (2015) Transgenic rabbits expressing ovine PrP are susceptible to scrapie. *PLoS Pathog* **11**, e1005077.

10 Chianini F, Fernandez-Borges N, Vidal E, Gibbard L, Pintado B, de Castro J, Priola SA, Hamilton S, Eaton SL, Finlayson J *et al.* (2012) Rabbits are not resistant to prion infection. *Proc Natl Acad Sci U S A* **109**, 5080–5085.

11 Beringue V, Vilotte JL & Laude H (2008) Prion agent diversity and species barrier. *Vet Res* **39**, 47.

12 Kraus A, Hoyt F, Schwartz CL, Hansen B, Artikis E, Hughson AG, Raymond GJ, Race B, Baron GS & Caughey B (2021) High-resolution structure and strain comparison of infectious mammalian prions. *Mol Cell* **81**, 4540–4551.e6.

13 Hoyt F, Standke HG, Artikis E, Schwartz CL, Hansen B, Li K, Hughson AG, Manca M, Thomas OR, Raymond GJ *et al.* (2022) Cryo-EM structure of anchorless RML prion reveals variations in shared motifs between distinct strains. *Nat Commun* **13**, 4005.

14 Manka SW, Wenborn A, Betts J, Joiner S, Saibil HR, Collinge J & Wadsworth JDF (2023) A structural basis for prion strain diversity. *Nat Chem Biol* **19**, 607–613.

15 Tixador P, Herzog L, Reine F, Jaumain E, Chapuis J, Le Dur A, Laude H & Beringue V (2010) The physical relationship between infectivity and prion protein aggregates is strain-dependent. *PLoS Pathog* **6**, e1000859.

16 Eskandari-Sedighi G, Cortez LM, Yang J, Daude N, Shmeit K, Sim V & Westaway D (2021) Quaternary structure changes for PrP(Sc) predate PrP(C) downregulation and neuronal death during progression of experimental scrapie disease. *Mol Neurobiol* **58**, 375–390.

17 Silveira JR, Raymond GJ, Hughson AG, Race RE, Sim VL, Hayes SF & Caughey B (2005) The most infectious prion protein particles. *Nature* **437**, 257–261.

18 Riesner D, Kellings K, Post K, Wille H, Serban H, Groth D, Baldwin MA & Prusiner SB (1996) Disruption of prion rods generates 10-nm spherical particles having high alpha-helical content and lacking scrapie infectivity. *J Virol* **70**, 1714–1722.

19 Laferriere F, Tixador P, Moudjou M, Chapuis J, Sibille P, Herzog L, Reine F, Jaumain E, Laude H, Rezaei H *et al.* (2013) Quaternary structure of pathological prion protein as a determining factor of strain-specific prion replication dynamics. *PLoS Pathog* **9**, e1003702.

20 Foliaki ST, Lewis V, Islam AMT, Ellett LJ, Senesi M, Finkelstein DI, Roberts B, Lawson VA, Adlard PA & Collins SJ (2019) Early existence and biochemical evolution characterise acutely synaptotoxic PrPSc. *PLoS Pathog* **15**, e1007712.

21 Igel-Egalon A, Bohl J, Moudjou M, Herzog L, Reine F, Rezaei H & Beringue V (2019) Heterogeneity and architecture of pathological prion protein assemblies: time to revisit the molecular basis of the prion replication process? *Viruses* **11**, 429.

22 Igel-Egalon A, Laferriere F, Moudjou M, Bohl J, Mezache M, Knapple T, Herzog L, Reine F, Jas-Duval C, Doumic M *et al.* (2019) Early stage prion assembly involves two subpopulations with different quaternary structures and a secondary templating pathway. *Commun Biol* **2**, 363.

23 Bohl J, Moudjou M, Herzog L, Reine F, Sailler F, Klute H, Halgand F, Van der Rest G, Boulard Y, Beringue V *et al.* (2023) The smallest infectious substructure encoding the prion strain structural determinant revealed by spontaneous dissociation of misfolded prion protein assemblies. *J Mol Biol* **435**, 168280.

24 Moreno JA & Telling GC (2017) Insights into mechanisms of transmission and pathogenesis from transgenic mouse models of prion diseases. *Methods Mol Biol* **1658**, 219–252.

25 Watts JC & Prusiner SB (2014) Mouse models for studying the formation and propagation of prions. *J Biol Chem* **289**, 19841–19849.

26 Groschup MH & Buschmann A (2008) Rodent models for prion diseases. *Vet Res* **39**, 32.

27 Chapuis J, Moudjou M, Reine F, Herzog L, Jaumain E, Chapuis C, Quadrio I, Boulliat J, Perret-Liaudet A, Dron M *et al.* (2016) Emergence of two prion subtypes in ovine PrP transgenic mice infected with human MM2-cortical Creutzfeldt-Jakob disease prions. *Acta Neuropathol Commun* **4**, 10.

28 Beringue V, Andreoletti V, Le Dur A, Essalmani R, Vilotte JL, Lacroux C, Reine F, Herzog L, Biacabè A-G, Baron T *et al.* (2007) A bovine prion acquires an epidemic bovine spongiform encephalopathy strain-like phenotype on interspecies transmission. *J Neurosci* **27**, 6965–6971.

29 Asante EA, Linehan JM, Desbruslais M, Joiner S, Gowland I, Wood AL, Welch J, Hill AF, Lloyd SE, Wadsworth JD *et al.* (2002) BSE prions propagate as either variant CJD-like or sporadic CJD-like prion

17424658, 2024, 22, Downloaded from https://febs.onlinelibrary.wiley.com/doi/10.1111/febs.17291 by Université de Versailles-Saint-Quentin-en-Yvelines, Wiley Online Library on [22/05/2025]. See the Terms and Conditions (https://onlinelibrary.wiley.com/terms-and-conditions) on Wiley Online Library for rules of use; OA articles are governed by the applicable Creative Commons License

strains in transgenic mice expressing human prion protein. *EMBO J* **21**, 6358–6366.
30 Bruce ME & Dickinson AG (1987) Biological evidence that scrapie agent has an independent genome. *J Gen Virol* **68**, 79–89.
31 Torres JM, Andreoletti O, Lacroux C, Prieto I, Lorenzo P, Larska M, Baron T & Espinosa JC (2011) Classical bovine spongiform encephalopathy by transmission of H-type prion in homologous prion protein context. *Emerg Infect Dis* **17**, 1636–1644.
32 Beringue V, Le Dur A, Tixador P, Reine F, Lepourry L, Perret-Liaudet A, Haik S, Vilotte JL, Fontes M & Laude H (2008) Prominent and persistent extraneural infection in human PrP transgenic mice infected with variant CJD. *PLoS One* **3**, e1419.
33 Le Dur A, Lai TL, Stinnakre MG, Laisne A, Chenais N, Rakotobe S, Passet B, Reine F, Soulier S, Herzog L *et al.* (2017) Divergent prion strain evolution driven by PrPC expression level in transgenic mice. *Nat Commun* **8**, 14170.
34 Collinge J & Clarke AR (2007) A general model of prion strains and their pathogenicity. *Science* **318**, 930–936.
35 Weissmann C, Li J, Mahal SP & Browning S (2011) Prions on the move. *EMBO Rep* **12**, 1109–1117.
36 Eigen M & Schuster P (1977) The hypercycle. A principle of natural self-organization, Part A: emergence of the hypercycle. *Naturwissenschaften* **64**, 541–565.
37 Igel-Egalon A, Laferriere F, Tixador P, Moudjou M, Herzog L, Reine F, Torres JM, Laude H, Rezaei H & Beringue V (2020) Crossing species barriers relies on structurally distinct prion assemblies and their complementation. *Mol Neurobiol* **57**, 2572–2587.
38 Makarava N & Baskakov IV (2013) The evolution of transmissible prions: the role of deformed templating. *PLoS Pathog* **9**, e1003759.
39 Legname G, Baskakov IV, Nguyen HO, Riesner D, Cohen FE, DeArmond SJ & Prusiner SB (2004) Synthetic mammalian prions. *Science* **305**, 673–676.
40 Choi JK, Cali I, Surewicz K, Kong Q, Gambetti P & Surewicz WK (2016) Amyloid fibrils from the N-terminal prion protein fragment are infectious. *Proc Natl Acad Sci U S A* **113**, 13851–13856.
41 Colby DW, Giles K, Legname G, Wille H, Baskakov IV, DeArmond SJ & Prusiner SB (2009) Design and construction of diverse mammalian prion strains. *Proc Natl Acad Sci U S A* **106**, 20417–20422.
42 Kim JI, Cali I, Surewicz K, Kong Q, Raymond GJ, Atarashi R, Race B, Qing L, Gambetti P, Caughey B *et al.* (2010) Mammalian prions generated from bacterially expressed prion protein in the absence of any mammalian cofactors. *J Biol Chem* **285**, 14083–14087.
43 Makarava N, Kovacs GG, Bocharova O, Savtchenko R, Alexeeva I, Budka H, Rohwer RG & Baskakov IV (2010) Recombinant prion protein induces a new transmissible prion disease in wild-type animals. *Acta Neuropathol* **119**, 177–187.
44 Makarava N, Savtchenko R, Alexeeva I, Rohwer RG & Baskakov IV (2016) New molecular insight into mechanism of evolution of mammalian synthetic prions. *Am J Pathol* **186**, 1006–1014.
45 Makarava N, Kovacs GG, Savtchenko R, Alexeeva I, Budka H, Rohwer RG & Baskakov IV (2011) Genesis of mammalian prions: from non-infectious amyloid fibrils to a transmissible prion disease. *PLoS Pathog* **7**, e1002419.
46 Kim C, Xiao X, Chen S, Haldiman T, Smirnovas V, Kofskey D, Warren M, Surewicz K, Maurer NR, Kong Q *et al.* (2018) Artificial strain of human prions created in vitro. *Nat Commun* **9**, 2166.
47 Moda F, Le TN, Aulic S, Bistaffa E, Campagnani I, Virgilio T, Indaco A, Palamara L, Andreoletti O, Tagliavini F *et al.* (2015) Synthetic prions with novel strain-specified properties. *PLoS Pathog* **11**, e1005354.
48 Groveman BR, Raymond GJ, Campbell KJ, Race B, Raymond LD, Hughson AG, Orru CD, Kraus A, Phillips K & Caughey B (2017) Role of the central lysine cluster and scrapie templating in the transmissibility of synthetic prion protein aggregates. *PLoS Pathog* **13**, e1006623.
49 Fernández-Borges N, Di Bari MA, Eraña H, Sánchez-Martín M, Pirisinu L, Parra B, Elezgarai SR, Vanni I, López-Moreno R, Vaccari G *et al.* (2018) Cofactors influence the biological properties of infectious recombinant prions. *Acta Neuropathol* **135**, 179–199.
50 Wang F, Wang X, Yuan CG & Ma J (2010) Generating a prion with bacterially expressed recombinant prion protein. *Science* **327**, 1132–1135.
51 Deleault NR, Harris BT, Rees JR & Supattapone S (2007) Formation of native prions from minimal components in vitro. *Proc Natl Acad Sci U S A* **104**, 9741–9746.
52 Jack K, Jackson GS & Bieschke J (2022) Essential components of synthetic infectious prion formation De novo. *Biomolecules* **12**, 1694.
53 Erana H, Diaz-Dominguez CM, Charco JM, Vidal E, Gonzalez-Miranda E, Perez-Castro MA, Pineiro P, Lopez-Moreno R, Sampedro-Torres-Quevedo C, Fernandez-Veiga L *et al.* (2023) Understanding the key features of the spontaneous formation of bona fide prions through a novel methodology that enables their swift and consistent generation. *Acta Neuropathol Commun* **11**, 145.
54 Erana H, Sampedro-Torres-Quevedo C, Charco JM, Diaz-Dominguez CM, Peccati F, San-Juan-Ansoleaga M, Vidal E, Goncalves-Anjo N, Perez-Castro MA, Gonzalez-Miranda E *et al.* (2024) A protein misfolding

17424658, 2024, 22, Downloaded from https://febs.onlinelibrary.wiley.com/doi/10.1111/febs.17291 by Université de Versailles-Saint-Quentin-en-Yvelines, Wiley Online Library on [22/05/2025]. See the Terms and Conditions (https://onlinelibrary.wiley.com/terms-and-conditions) on Wiley Online Library for rules of use; OA articles are governed by the applicable Creative Commons License

shaking amplification-based method for the spontaneous generation of hundreds of bona fide prions. *Nat Commun* **15**, 2112.
55 Cronier S, Beringue V, Bellon A, Peyrin JM & Laude H (2007) Prion strain- and species-dependent effects of antiprion molecules in primary neuronal cultures. *J Virol* **81**, 13794–13800.
56 Beringue V, Herzog L, Jaumain E, Reine F, Sibille P, Le Dur A, Vilotte JL & Laude H (2012) Facilitated cross-species transmission of prions in extraneural tissue. *Science* **335**, 472–475.
57 Moudjou M, Sibille P, Fichet G, Reine F, Chapuis J, Herzog L, Jaumain E, Laferriere F, Richard CA, Laude H *et al*. (2014) Highly infectious prions generated by a single round of microplate-based protein misfolding cyclic amplification. *MBio* **5**, e00829-13.
58 Igel-Egalon A, Moudjou M, Martin D, Busley A, Knapple T, Herzog L, Reine F, Lepejova N, Richard CA, Beringue V *et al*. (2017) Reversible unfolding of infectious prion assemblies reveals the existence of an oligomeric elementary brick. *PLoS Pathog* **13**, e1006557.
59 Zanusso G, Monaco S, Pocchiari M & Caughey B (2016) Advanced tests for early and accurate diagnosis of Creutzfeldt-Jakob disease. *Nat Rev Neurol* **12**, 325–333.
60 Wilham JM, Orru CD, Bessen RA, Atarashi R, Sano K, Race B, Meade-White KD, Taubner LM, Timmes A & Caughey B (2010) Rapid end-point quantitation of prion seeding activity with sensitivity comparable to bioassays. *PLoS Pathog* **6**, e1001217.
61 Cronier S, Gros N, Tattum MH, Jackson GS, Clarke AR, Collinge J & Wadsworth JD (2008) Detection and characterization of proteinase K-sensitive disease-related prion protein with thermolysin. *Biochem J* **416**, 297–305.
62 Owen JP, Maddison BC, Whitelam GC & Gough KC (2007) Use of thermolysin in the diagnosis of prion diseases. *Mol Biotechnol* **35**, 161–170.
63 Owen JP, Rees HC, Maddison BC, Terry LA, Thorne L, Jackman R, Whitelam GC & Gough KC (2007) Molecular profiling of ovine prion diseases by using thermolysin-resistant PrPSc and endogenous C2PrP fragments. *J Virol* **81**, 10532–10539.
64 Dron M, Moudjou M, Chapuis J, Salamat MK, Bernard J, Cronier S, Langevin C & Laude H (2010) Endogenous proteolytic cleavage of disease-associated prion protein to produce C2 fragments is strongly cell- and tissue-dependent. *J Biol Chem* **285**, 10252–10264.
65 Lewis V, Johanssen VA, Crouch PJ, Klug GM, Hooper NM & Collins SJ (2016) Prion protein "gamma-cleavage": characterizing a novel endoproteolytic processing event. *Cell Mol Life Sci* **73**, 667–683.
66 Lawson VA, Priola SA, Meade-White K, Lawson M & Chesebro B (2004) Flexible N-terminal region of prion protein influences conformation of protease-resistant prion protein isoforms associated with cross-species scrapie infection in vivo and in vitro. *J Biol Chem* **279**, 13689–13695.
67 Castilla J, Morales R, Saa P, Barria M, Gambetti P & Soto C (2008) Cell-free propagation of prion strains. *EMBO J* **27**, 2557–2566.
68 Stopschinski BE & Diamond MI (2017) The prion model for progression and diversity of neurodegenerative diseases. *Lancet Neurol* **16**, 323–332.
69 So RWL & Watts JC (2023) Alpha-synuclein conformational strains as drivers of phenotypic heterogeneity in neurodegenerative diseases. *J Mol Biol* **435**, 168011.
70 Le NT, Narkiewicz J, Aulic S, Salzano G, Tran HT, Scaini D, Moda F, Giachin G & Legname G (2015) Synthetic prions and other human neurodegenerative proteinopathies. *Virus Res* **207**, 25–37.
71 Lau HHC, Ingelsson M & Watts JC (2021) The existence of Abeta strains and their potential for driving phenotypic heterogeneity in Alzheimer's disease. *Acta Neuropathol* **142**, 17–39.
72 Nonno R, Di Bari MA, Cardone F, Vaccari G, Fazzi P, Dell'Omo G, Cartoni C, Ingrosso L, Boyle A, Galeno R *et al*. (2006) Efficient transmission and characterization of Creutzfeldt-Jakob disease strains in bank voles. *PLoS Pathog* **2**, e12.
73 Kimberlin RH, Walker CA & Fraser H (1989) The genomic identity of different strains of mouse scrapie is expressed in hamsters and preserved on reisolation in mice. *J Gen Virol* **70**, 2017–2025.
74 Kimberlin RH, Cole S & Walker CA (1987) Temporary and permanent modifications to a single strain of mouse scrapie on transmission to rats and hamsters. *J Gen Virol* **68**, 1875–1881.
75 Sandberg MK, Al-Doujaily H, Sharps B, Clarke AR & Collinge J (2011) Prion propagation and toxicity in vivo occur in two distinct mechanistic phases. *Nature* **470**, 540–542.
76 Halliez S, Reine F, Herzog L, Jaumain E, Haik S, Rezaei H, Vilotte JL, Laude H & Beringue V (2014) Accelerated, spleen-based titration of variant Creutzfeldt-Jakob disease infectivity in transgenic mice expressing human prion protein with sensitivity comparable to that of survival time bioassay. *J Virol* **88**, 8678–8686.
77 Bruce ME (1993) Scrapie strain variation and mutation. *Br Med Bull* **49**, 822–838.
78 Race R & Chesebro B (1998) Scrapie infectivity found in resistant species. *Nature* **392**, 770.
79 Yoshioka M, Imamura M, Okada H, Shimozaki N, Murayama Y, Yokoyama T & Mohri S (2011) Sc237 hamster PrPSc and Sc237-derived mouse PrPSc

17424658, 2024, 22, Downloaded from https://febs.onlinelibrary.wiley.com/doi/10.1111/febs.17291 by Université de Versailles-Saint-Quentin-en-Yvelines, Wiley Online Library on [22/05/2025]. See the Terms and Conditions (https://onlinelibrary.wiley.com/terms-and-conditions) on Wiley Online Library for rules of use; OA articles are governed by the applicable Creative Commons License

generated by interspecies in vitro amplification exhibit distinct pathological and biochemical properties in tga20 transgenic mice. *Microbiol Immunol* **55**, 331–340.
80 Sigurdson CJ, Manco G, Schwarz P, Liberski P, Hoover EA, Hornemann S, Polymenidou M, Miller MW, Glatzel M & Aguzzi A (2006) Strain fidelity of chronic wasting disease upon murine adaptation. *J Virol* **80**, 12303–12311.
81 Jeffrey M & Gonzalez L (2007) Classical sheep transmissible spongiform encephalopathies: pathogenesis, pathological phenotypes and clinical disease. *Neuropathol Appl Neurobiol* **33**, 373–394.
82 Baron T, Bencsik A, Vulin J, Biacabe AG, Morignat E, Verchere J & Betemps D (2008) A C-terminal protease-resistant prion fragment distinguishes ovine "CH1641-like" scrapie from bovine classical and L-type BSE in ovine transgenic mice. *PLoS Pathog* **4**, e1000137.
83 Biacabe AG, Jacobs JG, Bencsik A, Langeveld JP & Baron TG (2007) H-type bovine spongiform encephalopathy: complex molecular features and similarities with human prion diseases. *Prion* **1**, 61–68.
84 Zou WQ, Capellari S, Parchi P, Sy MS, Gambetti P & Chen SG (2003) Identification of novel proteinase K-resistant C-terminal fragments of PrP in Creutzfeldt-Jakob disease. *J Biol Chem* **278**, 40429–40436.
85 Linsenmeier L, Altmeppen HC, Wetzel S, Mohammadi B, Saftig P & Glatzel M (2017) Diverse functions of the prion protein - does proteolytic processing hold the key? *Biochim Biophys Acta* **1864**, 2128–2137.
86 Munoz-Montesino C, Larkem D, Barbereau C, Igel-Egalon A, Truchet S, Jacquet E, Nhiri N, Moudjou M, Sizun C, Rezaei H *et al.* (2020) A seven-residue deletion in PrP leads to generation of a spontaneous prion formed from C-terminal C1 fragment of PrP. *J Biol Chem* **295**, 14025–14039.
87 Miller MB, Geoghegan JC & Supattapone S (2011) Dissociation of infectivity from seeding ability in prions with alternate docking mechanism. *PLoS Pathog* **7**, e1002128.
88 Vanni I, Migliore S, Cosseddu GM, Di Bari MA, Pirisinu L, D'Agostino C, Riccardi G, Agrimi U & Nonno R (2016) Isolation of a defective prion mutant from natural scrapie. *PLoS Pathog* **12**, e1006016.
89 Vanni I, Pirisinu L, Acevedo-Morantes C, Kamali-Jamil R, Rathod V, Di Bari MA, D'Agostino C, Marcon S, Esposito E, Riccardi G *et al.* (2020) Isolation of infectious, non-fibrillar and oligomeric prions from a genetic prion disease. *Brain* **143**, 1512–1524.
90 Supattapone S, Bosque P, Muramoto T, Wille H, Aagaard C, Peretz D, Nguyen HO, Heinrich C, Torchia M, Safar J *et al.* (1999) Prion protein of 106 residues creates an artifical transmission barrier for prion replication in transgenic mice. *Cell* **96**, 869–878.
91 Wang LQ, Zhao K, Yuan HY, Wang Q, Guan Z, Tao J, Li XN, Sun Y, Yi CW, Chen J *et al.* (2020) Cryo-EM structure of an amyloid fibril formed by full-length human prion protein. *Nat Struct Mol Biol* **27**, 598–602.
92 Rezaei H, Marc D, Choiset Y, Takahashi M, Hui Bon Hoa G, Haertle T, Grosclaude J & Debey P (2000) High yield purification and physico-chemical properties of full-length recombinant allelic variants of sheep prion protein linked to scrapie susceptibility. *Eur J Biochem* **267**, 2833–2839.
93 Breydo L, Makarava N & Baskakov IV (2008) Methods for conversion of prion protein into amyloid fibrils. *Methods Mol Biol* **459**, 105–115.
94 Torrent J, Martin D, Noinville S, Yin Y, Doumic M, Moudjou M, Béringue V & Rezaei H (2019) Pressure reveals unique conformational features in prion protein fibril diversity. *Sci Rep* **9**, 2802.
95 Prusiner SB, Scott M, Foster D, Pan KM, Groth D, Mirenda C, Torchia M, Yang SL, Serban D, Carlson GA *et al.* (1990) Transgenetic studies implicate interactions between homologous PrP isoforms in scrapie prion replication. *Cell* **63**, 673–686.
96 Martin D, Reine F, Herzog L, Igel-Egalon A, Aron N, Michel C, Moudjou M, Fichet G, Quadrio I, Perret-Liaudet A *et al.* (2021) Prion potentiation after life-long dormancy in mice devoid of PrP. *Brain Commun* **3**, fcab092.
97 Al-Dybiat I, Moudjou M, Martin D, Reine F, Herzog L, Truchet S, Berthon P, Laude H, Rezaei H, Andréoletti O *et al.* (2019) Prion strain-dependent tropism is maintained between spleen and granuloma and relies on lymphofollicular structures. *Sci Rep* **9**, 14656.
98 Markus RA, Frank J, Groshen S & Azen SP (1995) An alternative approach to the optimal design of an LD50 bioassay. *Stat Med* **14**, 841–852.
99 Bueler H, Aguzzi A, Sailer A, Greiner RA, Autenried P, Aguet M & Weissmann C (1993) Mice devoid of PrP are resistant to scrapie. *Cell* **73**, 1339–1347.
100 Fraser H & Dickinson AG (1968) The sequential development of the brain lesion of scrapie in three strains of mice. *J Comp Pathol* **78**, 301–311.
101 Fraser H & Dickinson AG (1973) Scrapie in mice. Agent-strain differences in the distribution and intensity of grey matter vacuolation. *J Comp Pathol* **83**, 29–40.
102 Beringue V, Bencsik A, Le Dur A, Reine F, Lan Lai T, Chenais N, Tilly G, Biacabè A-G, Baron T, Vilotte JL *et al.* (2006) Isolation from cattle of a prion strain distinct from that causing bovine spongiform encephalopathy. *PLoS Pathog* **2**, 956–963.
103 Beringue V, Herzog L, Reine F, Le Dur A, Casalone C, Vilotte JL & Laude H (2008) Transmission of atypical bovine prions to mice transgenic for human prion protein. *Emerg Infect Dis* **14**, 1898–1901.

17424658, 2024, 22, Downloaded from https://febs.onlinelibrary.wiley.com/doi/10.1111/febs.17291 by Université de Versailles-Saint-Quentin-en-Yvelines, Wiley Online Library on [22/05/2025]. See the Terms and Conditions (https://onlinelibrary.wiley.com/terms-and-conditions) on Wiley Online Library for rules of use; OA articles are governed by the applicable Creative Commons License

104 Bruce ME, Boyle A, Cousens S, McConnell I, Foster J, Goldmann W & Fraser H (2002) Strain characterization of natural sheep scrapie and comparison with BSE. *J Gen Virol* **83**, 695–704.
105 Nicot S & Baron T (2011) Strain-specific barriers against bovine prions in hamsters. *J Virol* **85**, 1906–1908.

Supporting information

Additional supporting information may be found online in the Supporting Information section at the end of the article.

Fig. S1. Flow diagram describing the protocol used to prepare recombinant PrP assemblies.
Table S1. Absence of prion disease in tg7 mice after intracerebral inoculation of monomers from hamster, mouse, and human recombinant PrP.
Table S2. List of the anti-PrP antibodies used in the study.
Table S3. Transmission of animal prions to tg7 mice by intracerebral route.

17424658, 2024, 22, Downloaded from https://febs.onlinelibrary.wiley.com/doi/10.1111/febs.17291 by Université de Versailles-Saint-Quentin-en-Yvelines, Wiley Online Library on [22/05/2025]. See the Terms and Conditions (https://onlinelibrary.wiley.com/terms-and-conditions) on Wiley Online Library for rules of use; OA articles are governed by the applicable Creative Commons License